Main Manuscript for:

Histone deacetylation and cytosine methylation compartmentalize heterochromatic regions in the genome organization of *Neurospora crassa*

Ashley W. Scadden[1], Alayne S. Graybill[1], Clayton Hull-Crew[1], Tiffany J. Lundberg[1], Nickolas M. Lande[1], and Andrew D. Klocko[1]*

[1]University of Colorado Colorado Springs, Department of Chemistry & Biochemistry, Colorado Springs, CO 80918, USA

***Corresponding Author:** Andrew D. Klocko, email: aklocko@uccs.edu

Author Contributions: A.W.S and A.D.K. designed research; A.W.S., A.S.G., C.H-C., T.J.L., N.M.L., and A.D.K. performed research; A.W.S., A.S.G., C.H-C., T.J.L., N.M.L., and A.D.K. analyzed data; and A.W.S., A.S.G., C.H-C., T.J.L., N.M.L., and A.D.K. wrote the paper.

Competing Interest Statement: The authors declare no conflict of interest.

Classification: Biological Sciences, Genetics

Keywords: histone deacetylation, genome organization, heterochromatin, Hi-C, cytosine methylation

Abstract

Chromosomes must correctly fold in eukaryotic nuclei for proper genome function. Eukaryotic organisms hierarchically organize their genomes, including in the fungus *Neurospora crassa*, where chromatin fiber loops compact into Topologically Associated Domain (TAD)-like structures formed by heterochromatic region aggregation. However, insufficient data exists on how histone post-translational modifications, including acetylation, affect genome organization. In Neurospora, the HCHC complex (comprised of the proteins HDA-1, CDP-2, HP1, and CHAP) deacetylates heterochromatic nucleosomes, as loss of individual HCHC members increases centromeric acetylation and alters the methylation of cytosines in DNA. Here, we assess if the HCHC complex affects genome organization by performing Hi-C in strains deleted of the *cdp-2* or *chap* genes. CDP-2 loss increases intra- and inter-chromosomal heterochromatic region interactions, while loss of CHAP decreases heterochromatic region compaction. Individual HCHC mutants exhibit different patterns of histone post-translational modifications genome-wide: without CDP-2, heterochromatic H4K16 acetylation is increased, yet smaller heterochromatic regions lose H3K9 trimethylation and gain inter-heterochromatic region interactions; CHAP loss produces minimal acetylation changes but increases heterochromatic H3K9me3 enrichment. Loss of both CDP-2 and the DIM-2 DNA methyltransferase causes extensive genome disorder, as heterochromatic-euchromatic contacts increase despite additional H3K9me3 enrichment. Our results highlight how the increased cytosine methylation in HCHC mutants ensures genome compartmentalization when heterochromatic regions become hyperacetylated without HDAC activity.

Significance Statement

The mechanisms driving chromosome organization in eukaryotic nuclei, including in the filamentous fungus *Neurospora crassa*, are currently unknown, but histone post-translational modifications may be involved. Histone proteins can be acetylated to form active euchromatin while histone deacetylases (HDACs) remove acetyl marks to form silent heterochromatin; these heterochromatic regions cluster, forming strong interactions, in Neurospora genome organization. Here, we show that mutants of a heterochromatin-specific HDAC, HCHC, increase heterochromatic histone acetylation genome-wide and contact probability between distant heterochromatic loci. HCHC loss also impacts cytosine methylation, and in strains lacking both the HCHC and cytosine methylation, heterochromatic regions interact more with euchromatin. Our results suggest cytosine methylation normally functions to segregate silent and active loci when heterochromatic acetylation increases.

Main Text

Introduction

Chromosomes must correctly fold in eukaryotic nuclei for proper genome function, including for transcription regulation (1–5). This genome organization includes the subnuclear compartmentalization of chromatin (2, 5) where the silent heterochromatin aggregates at the nuclear periphery to prevent RNA polymerase binding while active euchromatin is centrally localized and accessible to the transcription machinery (6–9). In euchromatin, long-range loops form between promoters and distant regulatory sequences, including enhancers or silencers, for transcriptional control (3, 10). Genome organization is frequently disrupted in human cancers, where promoters hijack regulatory sequences for improper gene expression (11–13). Given the direct connection between genome organization and function, there is a critical need to understand the factors involved in wild type (WT) chromosome folding.

Genome organization is assessed by chromosome conformation capture with high throughput sequencing (Hi-C), in which crosslinked chromatin is restriction enzyme digested and ligated to physically connect interacting DNA strands in a single DNA molecule; the updated *in situ* Hi-C protocol ligates interacting chromatin in the nucleus, thereby generating more accurate genome organization contact probability matrices (14–16). Hi-C has shown that eukaryotic genomes are hierarchically organized, where histone octamers wrap ~146 basepairs (bp) of DNA to form the nucleosomes comprising chromatin fiber globules ("loops") (17, 18). Globules compact into Topologically Associated Domains (TADs), where chromatin internal to the TAD is more apt to interact (15, 19–21). TADs of similar transcriptional states are compartmentalized, while individual metazoan chromosomes isolate into territories (6, 14, 15, 22–25).

Filamentous fungi, like *Neurospora crassa*, are excellent model organisms for understanding eukaryotic genome organization (16, 26–28). The predominantly haploid Neurospora genome, typical among fungi, is small (4.1×10^7 bp) (29), which allows for cost-efficient genomic sequencing experiments. The Neurospora genome contains both euchromatic and heterochromatic loci, with the latter subdivided into permanently-silent constitutive heterochromatin comprised of gene-poor, repetitive, adenine-thymine (AT)-rich DNA, and temporarily-silent facultative heterochromatin covering gene-rich regions (29–32); each type is marked by specific histone post-translational modifications (PTMs). Neurospora constitutive heterochromatin is

78 enriched with trimethylation of lysine 9 on histone H3 (H3K9me3, catalyzed by the **D**IM-5/-7/-9, **C**UL4,
79 **D**DB1*dim-8* **C**omplex [DCDC]) and cytosine methylation (5^{m}C), while the di- or trimethylation of lysine 27 on
80 histone H3 (H3K27me2/3) or the ASH1-dependent di-methylation of lysine 36 on histone H3 (H3K36me2)
81 demarcates facultative heterochromatin (30–38). Histone lysines in euchromatin are extensively acetylated
82 by histone acetyltransferases (HATs), including on histone H3 lysine 9 (H3K9ac) or histone H4 lysine 16
83 (H4K16ac) (39–41). Unlike metazoans, the machinery catalyzing histone PTMs or 5^{m}C in Neurospora is
84 simplistic, non-redundant, and not required for viability, promoting the use of Neurospora for understanding
85 chromatin function (32, 38, 42). Notably, the Neurospora genome is compacted and organized similarly to
86 metazoan genomes, with a comparable genome size to nuclear volume ratio (16). Neurospora chromosomes
87 ("Linkage Groups" [LG]) form TAD-like structures, also known as "Regional Globule Clusters", in which the
88 heterochromatic regions flanking euchromatin aggregate, forming loops that cluster several euchromatic
89 globules together in an uninsulated manner (16, 26, 27). However, as opposed to the robust chromosome
90 territories in metazoans (1, 22, 24, 25), fungal chromosomes form a Rabl conformation, in which
91 centromeres bundle independently from telomere clusters at the nuclear periphery (16, 26–28, 43), as
92 directly observed in Neurospora (26–28); this Rabl structure allows for weak chromosome territories with
93 extensive inter-chromosomal contacts.

94 Chromatin compartmentalization may depend on individual histone PTMs. Since specific histone PTMs
95 are known to define chromatin transcriptional status and accessibility (18, 44–46), histone PTMs may also
96 be necessary for segregating euchromatin from heterochromatin in the nucleus. Recent reports detail how
97 heterochromatic histone PTMs, or their cognate binding partners, organize eukaryotic genomes. This
98 includes H3K9me3 and Heterochromatin Protein-1 (HP1), which compact heterochromatic regions during
99 fungal asexual growth and facilitate pericentromere clustering during Drosophila zygote genome activation
100 (27, 43, 47). In addition, sub-telomeric H3K27me2/3 helps telomere clusters associate with the nuclear
101 periphery in Neurospora (26). However, little information exists about the roles of other histone PTMs,
102 including histone acetylation.

103 Classically, acetylated histone tails denote open chromatin, as the euchromatic regions of fungi, fruit flies,
104 mice, and humans are highly acetylated (33, 48–57). In contrast, heterochromatin is typically devoid of

105 histone acetylation, as histone deacetylase (HDAC) complexes remove acetyl marks from silent loci (33, 39,
106 40, 58). Changes in acetylation enrichment impact genome organization, including the interactions between
107 promoters and enhancers. Differential acetylation of lysine 27 on histone H3 (H3K27ac) across enhancers is
108 observed during the differentiation of human epidermal cells (59) and mouse adipocyte cells (60). Histone
109 acetylation changes also occur throughout the cell cycle, as mitotic chromosomes are globally
110 hypoacetylated, which forms dense chromosomal structures allowing separation into daughter cells (61–
111 65). H3K27 within promoters and enhancers is deacetylated during mitosis but rapidly re-acetylated in G1
112 for activating transcription and reforming TADs (66, 67). Further, the BRD4-NUT novel oncogenic protein
113 recruits the HAT P300 to create hyperacetylated Mega-domains that aggregate into a transcriptionally
114 activated sub-compartment (68); phase-separation might promote sub-compartment formation (69).
115 However, it is unknown how HDAC activity affects fungal chromosome conformation.

116 *Neurospora crassa* encodes four class II HDACs (HDA-1 to HDA-4; class characterization based on
117 primary structure conservation), with HDA-1 impacting heterochromatin (41, 58). HDA-1 is a component of
118 the four-member HCHC complex, comprised of the proteins HDA-1, CDP-2 (***C***hromo***d***omain ***P***rotein-***2***), HP1,
119 and CHAP (***C***DP-2 and ***H***DA-1 ***A***ssociated ***P***rotein) (39, 40). HDA-1 is the deacetylase catalytic subunit, HP1
120 binding to H3K9me3 recruits the complex to heterochromatin, CDP-2 mediates protein interactions between
121 HP1 and HDA-1, and CHAP binds to AT-rich DNA in constitutive heterochromatin using two AT hook domains
122 (39, 40). Both CDP-2 and CHAP recruit HDA-1 to heterochromatic genomic loci (39). Strains deleted of the
123 genes *cdp-2*, *chap*, or *hda-1* have increased histone acetylation at select heterochromatic loci, as assessed by
124 Chromatin Immunoprecipitation (ChIP) quantitative PCR, although genome-wide changes are unknown
125 (40). Smaller heterochromatic regions in HCHC mutants lose $5^{m}C$ but larger regions, including centromeres,
126 gain $5^{m}C$ by increasing recruitment of DIM-2, the only DNA methyltransferase encoded in Neurospora (39).

127 Here, we show the HCHC complex impacts genome organization using Δ*cdp-2* and Δ*chap* deletion strains.
128 CDP-2 loss increases intra- and inter-chromosomal heterochromatic region contacts, while deletion of CHAP
129 reduces heterochromatic region compaction. Heterochromatic regions gain H4K16ac but not H3K9ac in a
130 Δ*cdp-2* strain, while a Δ*chap* strain has little H4K16ac change. Smaller heterochromatic regions lose

131 H3K9me3 in a Δ*cdp-2* strain, causing contact promiscuity between silent loci. A Δ*cdp-2*;Δ*dim-2* double mutant
132 devoid of 5^{m}C and HCHC activity gains H3K9me3 but loses heterochromatin – euchromatin
133 compartmentalization, suggesting global genome disorder. We conclude that histone deacetylation is
134 required for Neurospora genome organization, but if histones become hyperacetylated, 5^{m}C helps maintain
135 segregation of heterochromatin from euchromatin.
136

137 **Results**

138 *Genome organization changes in strains deleted of either HCHC component CDP-2 or CHAP*

139 The genome of the wild type (WT) *Neurospora crassa* strain N150 (74-OR23-IVA [Fungal Genetic Stock
140 Center #2489]) is organized by heterochromatin aggregates, which form TAD-like structures (Figure 1A)
141 (16, 26–28). Heterochromatic regions in Neurospora depend on the HDAC HCHC for deacetylation of histone
142 tails, transcriptional silencing, and a normal 5^{m}C distribution (40). To understand if the HCHC complex also
143 organizes the Neurospora genome, we examined strains independently deleted of the genes encoding CDP-
144 2 (Δ*cdp-2*) or CHAP (Δ*chap*) by *in situ* Hi-C. We chose CDP-2 and CHAP given the unique domains predicted
145 by their primary protein structures and how their actions are epistatic to HDA-1 (39, 40), hypothesizing that
146 we could observe more nuanced differences in genome organization upon loss of HCHC activity to clarify the
147 individual roles of CDP-2 and CHAP, instead of only assessing the impact of HDA-1 catalytic activity loss. We
148 independently performed chromatin-specific *in situ* Hi-C (16) with *Dpn*II (recognition sequence ^GATC) to
149 assess euchromatic contacts, or *Mse*I (T^TAA) to examine heterochromatic interactions, on Δ*cdp-2* and Δ*chap*
150 strains. All Hi-C experiments reported in this manuscript are generated from populations of actively growing
151 cells containing asynchronous nuclei, most of which are typically in interphase stages of the cell cycle with
152 less than 5% mitotic nuclei (70, 71). Our replicate *in situ* Hi-C libraries are highly reproducible (Figures S1,
153 S2), allowing similar restriction enzyme datasets to be merged. This produced high quality *Dpn*II Δ*cdp-2*
154 (~35.4 million [M] valid read pairs) and Δ*chap* (~8.7M valid read pairs), as well as *Mse*I Δ*cdp-2* (~13.9M
155 valid read pairs) and Δ*chap* (~4.8M valid read pairs) datasets; total and valid read counts are provided in
156 Supplemental Table S1. The merged *Dpn*II datasets presented are Knight-Ruiz (KR) corrected to limit
157 experimental bias (22, 72, 73), while *Mse*I datasets show raw read counts, since KR correction improperly

158 removes heterochromatin signal upon bin averaging, possibly due to the discrepancy of *Mse*I sites between
159 AT-rich heterochromatin and GC-rich euchromatin (16).

160 The *Dpn*II and *Mse*I Δ*cdp-2* contact probability heatmaps of a single chromosome (Figures 1B) look
161 comparable to WT *Dpn*II or *Mse*I Hi-C datasets with nearly identical valid read numbers (Figure 1A), but upon
162 closer examination, the Δ*cdp-2* dataset has increased interactions between distant heterochromatic regions.
163 Specifically, the LG II centromere forms prominent interactions with heterochromatic regions up to three
164 Megabases (Mb) distant in the heterochromatin specific *Mse*I heatmap (Figure 1B, black arrowheads), while
165 heterochromatic regions form fewer contacts with nearby euchromatin (Figure 1B, open arrowheads). These
166 effects are seen across all seven Neurospora chromosomes (Figures S3). To highlight changes in a Δ*cdp-2*
167 strain, we directly compared the WT and Δ*cdp-2 Dpn*II or *Mse*I Hi-C contact probability matrices. In
168 comparison heatmaps, the strong increases between centromeres and distant heterochromatic regions in a
169 Δ*cdp-2* strain are among the most prominent across LG II (Figure 1C) and all seven Neurospora LGs (Figure
170 S4). At a high resolution, the Δ*cdp-2* centromeric chromatin shows increased contacts, as evident by the LG
171 II centromere having a strong red diagonal indicative of increased contacts between centromeric
172 nucleosomes, in addition to having more intense interactions with distant H3K9me3-marked constitutive
173 heterochromatic regions (Figure 1D). In fact, each heterochromatic region in Δ*cdp-2 Mse*I datasets has
174 increased local interactions on the diagonal that depletes heterochromatic-euchromatic contacts (Figures
175 1B-C, S4). Quantification of strongly changed contacts between WT and Δ*cdp-2 Mse*I datasets showed that
176 most H3K9me3 enriched bins had stronger ($\log_2 \geq 2.0$) interactions with another H3K9me3 enriched bin;
177 few H3K9me3 enriched bins had strong interaction changes with bins enriched for euchromatic marks in
178 *Mse*I datasets (Figure 1E). The contact paucity in off diagonal euchromatic interactions in a Δ*cdp-2 Mse*I
179 dataset, relative to WT (Figure 1C, above diagonal), could indicate chromatin in TAD-like structures interact
180 less or is due to fewer euchromatic *Mse*I sites for Hi-C ligation (16) coupled with increased heterochromatic
181 contacts (Figure 1C). As evident in *Dpn*II datasets, interactions of distant euchromatic regions are globally
182 decreased, including between the left and right chromosome arms and between distant TAD-like structures
183 (Figure 1C). However, individual bins quantitatively have strongly changed interactions when comparing
184 WT and Δ*cdp-2 Dpn*II datasets, as more bins enriched for two euchromatic histone PTMs, H3K27ac and SET-

185 2-specific H3K36me2 (33), were increased, although some H3K9me3 marked bins interacted more with
186 euchromatin (Figure 1E). All told, CDP-2 loss increases constitutive heterochromatin interactions which
187 alters the normal conformation of Neurospora chromosomes.

188 Next, we examined the genome organization of a Δ*chap* strain by *Dpn*II and *Mse*I Hi-C. The Δ*chap* data
189 has fewer valid reads, with ~four-fold less valid reads in the Δ*chap Dpn*II dataset and ~three-fold less valid
190 reads in the Δ*chap Mse*I dataset, relative to the Δ*cdp-2* datasets (Supplemental Table S1). However, sufficient
191 data exists in Δ*chap* datasets to allow comparison with normalized WT datasets containing similar valid read
192 numbers, so the impact of CHAP loss can be assessed. Examination of single chromosomes show how the
193 Δ*chap Dpn*II and *Mse*I Hi-C datasets appear devoid of most strong long-range contacts (Figures 1F, S5). In
194 each chromosome, more distant contacts are rarer upon CHAP loss; an enhanced image of the right arm of
195 LG II highlights that regional interactions still form in both *Dpn*II and *Mse*I datasets (Figure S6). When
196 comparing WT and Δ*chap* datasets, heterochromatic regions on all LGs exhibit reduced internal compaction,
197 and fewer contacts between heterochromatic regions are observed (Figures 1G; S6B, arrowheads; S7). Also
198 apparent are the decreased interactions between the TAD-like Regional Globule Clusters (16) in the Δ*chap*
199 *Dpn*II data, which may stem from the slight increase in on-diagonal, local euchromatic interactions (Figures
200 1G, S6-S7). Quantification of strongly increased contacts in Δ*chap Dpn*II or *Mse*I datasets relative to WT
201 shows that interactions between bins enriched for the euchromatic marks H3K27ac and SET-2-specific
202 H3K36me2 (33) are the most frequently increased when CHAP is lost (Figure 1E).

203 Similarly, loss of CDP-2 and CHAP impact the inter-chromosomal clustering of heterochromatic regions
204 across the entire Neurospora genome. As shown in raw *Mse*I and KR-corrected *Dpn*II contact probability
205 heatmaps of a Δ*cdp-2* strain, or when these Δ*cdp-2* data are compared to normalized WT contact matrices,
206 Δ*cdp-2* centromeres gain interactions with the interspersed heterochromatic regions across all seven LGs,
207 concomitantly weakening the inter-chromosomal centromere interactions and the contacts between
208 centromere-proximal euchromatin (Figures S8-S9), although these reductions may result if one dataset
209 (Δ*cdp-2*) has more heterochromatin contacts when comparing datasets with equal valid read pairs. The Δ*cdp-*
210 *2 Dpn*II Hi-C data have stronger inter-chromosomal arm contacts (Figure S9); similar changes are observed
211 in KR-corrected *Mse*I data and raw *Dpn*II data when comparing WT and Δ*cdp-2* contact matrices (Figure

212 S10A). Examination of the interactions between two chromosomes, LG II and LG III, in Δ*cdp-2 Mse*I Hi-C
213 contact heatmaps show the gain of centromeric and interspersed heterochromatic region contacts and the
214 concomitant reduction of contacts between silent and active chromatin (Figure S8A). Plotting the inter-
215 chromosomal interaction changes of WT and Δ*cdp-2 Mse*I datasets between LG II and LG III highlight how
216 distant heterochromatic regions between chromosomes are more apt to interact with the centromere bundle
217 (Figure 2A). Decreased contacts include the inter-centromeric and pericentromeric euchromatin (Figure
218 2A). CHAP loss reduces heterochromatic interactions across the Neurospora genome, with few inter-
219 chromosomal heterochromatic contacts observed in Δ*chap Mse*I contact matrices (Figure S11), and
220 prominent reductions in centromeric contacts that are independent of matrix correction when WT and Δ*chap*
221 *Mse*I data is compared (Figures S9B, S10B). A plot of the interactions between LG II and LG III in Δ*chap* shows
222 the paucity of inter-chromosomal constitutive heterochromatic contacts (Figure S11A), which is highlighted
223 when comparing WT and Δ*chap Mse*I Hi-C data (Figure 2B). The decrease in heterochromatin bundling
224 compromises the inter-chromosomal arm interactions characteristic of the Rabl conformation (28), as
225 reduced euchromatin interactions across the left and right chromosomal arms are evident in a WT and Δ*chap*
226 *Dpn*II Hi-C comparison (Figure S10B). Quantification of the strongest inter-chromosomal interaction gains
227 between histone PTM-enriched bins in a Δ*cdp-2 Mse*I dataset, relative to WT, shows 81.5% of H3K9me3
228 enriched bins gain interactions, but few H3K9me3-enriched bins gain strong contacts with bins enriched
229 with euchromatic marks, such as H3K27ac (Figure 2C, left). The Δ*cdp-2 Dpn*II Hi-C data show changes in
230 strong interactions between bins enriched with H3K9me3 and euchromatic histone PTMs, such as H3K27ac
231 and SET-2 specific H3K36me2, or between two euchromatic enriched bins (Figure 2C, right). In contrast,
232 Δ*chap Mse*I and *Dpn*II Hi-C datasets have minimal gains in interactions relative to WT, independent of histone
233 PTMs, consistent with the loss of CHAP reducing heterochromatic interactions (Figure 2C). To highlight the
234 differential effects of CDP-2 and CHAP loss on genome organization, we compared equal numbers of valid
235 reads to highlight interaction changes in a Δ*chap* strain relative to a Δ*cdp-2* strain. Here, the decreases in
236 heterochromatin compaction, inter-heterochromatic region contacts, and contacts between chromosomal
237 arms, with the concomitant increase in local euchromatic interactions that occur upon loss of CHAP, relative
238 to the CDP-2 changes, is evident (Figure S12). All told, our Δ*cdp-2* and Δ*chap* Hi-C data reveal the differential

239 effects on genome organization by individual members of a histone deacetylase complex.

240

241 *Histone acetylation changes in single deletion strains of the HCHC components CDP-2 and CHAP*

242 To understand how the genome organization changes caused by deficient HCHC function affects genome
243 function, we wished to correlate changes in Hi-C contact probability to any genome-wide changes in histone
244 acetylation in Δ*cdp-2* and Δ*chap* strains. However, no Chromatin Immunoprecipitation-sequencing (ChIP-
245 seq) datasets of HCHC mutants were publicly available, as recent publications only used ChIP qPCR to
246 conclude that heterochromatic loci in HCHC deficient strains are hyperacetylated (40). Therefore, we
247 performed two ChIP-seq replicates of histone acetylation on two lysine residues, K9 on histone H3 (H3K9ac)
248 and K16 on histone H4 (H4K16ac), in Δ*cdp-2* and WT strains; we also performed H4K16ac ChIP-seq on a
249 Δ*chap* strain. Both H3K9ac and H4K16ac were proposed as targets for deacetylation by the HCHC complex
250 (40). Our H3K9ac and H4K16ac ChIP-seq replicates are qualitatively reproducible in each strain (Figure S13,
251 S14), so we merged H3K9ac or H4K16ac replicates for Integrative Genome Viewer (IGV) display (74); all
252 ChIP-seq data reported in this manuscript are normalized by Reads Per Kilobase per Million reads (RPKM)
253 to ensure proper comparison between experiments, although the use of spike-in DNA (75–77) might have
254 detected additional enrichment changes. Consistent with published ChIP qPCR, CDP-2 loss caused an
255 increase in H4K16ac enrichment only in AT-rich heterochromatic regions but minimally effected H3K9ac
256 levels across Neurospora chromosomes (Figure 3A, top). Closer examination of the LG II right arm highlights
257 how each H3K9me3-marked heterochromatic region gains H4K16ac, but not H3K9ac, in a Δ*cdp-2* strain
258 (Figure 3A, bottom, arrowheads), while euchromatic acetylation of either histone lysine is relatively
259 unchanged (Figure 3A). In contrast, CHAP loss had little effect on H4K16ac enrichment within constitutive
260 heterochromatic or genic regions (Figure S15A).

261 These acetylation changes are highlighted by average enrichment plots and heatmaps of normalized
262 H4K16ac and H3K9ac datasets across H3K9me3-enriched heterochromatic regions and genes. By aligning
263 heterochromatic region centers and ordering these silent regions by length, we observe that essentially all
264 AT-rich heterochromatic regions, independent of size, have substantial increases in H4K16ac enrichment in
265 a Δ*cdp-2* strain relative to a WT strain (Figure 3B). Similar gains in H4K16ac in a Δ*cdp-2* strain are seen when

266 each heterochromatic region is scaled to 10 kb and ordered by region length (Figure S16A), while the H3K9ac
267 enrichment in Δ*cdp-2* heterochromatin may be slightly lower than that of WT (Figure S17A). In contrast, this
268 approach shows minimal gains of heterochromatic H4K16ac in a Δ*chap* strain (Figure S15B). When assessing
269 H4K16ac and H3K9ac over genes (scaled to 2.5 kb), a Δ*cdp-2* strain has minimal H4K16ac reduction, while
270 H3K9ac slightly shifts towards the 3' end of genes, relative to WT (Figures S16B and S17B); a Δ*chap* strain
271 has a nominal decrease in genic H4K16ac (Figure S15C). To visualize the H4K16ac and H3K9ac deposition
272 changes, we plotted the normalized, averaged signal of each region with boxplots. The heterochromatic
273 regions in Δ*cdp-2* have robust increases in H4K16ac signal relative to WT (Figure S16C), while H3K9ac
274 enrichment is generally decreased (Figure S17C), although some regions in either dataset go against these
275 trends. Considering genic acetylation, a Δ*cdp-2* strain has a small but statistically significant H4K16ac
276 decrease (Figure S16D) and H3K9ac increase (Figure S17D). Together, HCHC loss differentially effects
277 enrichment of histone acetylation across the Neurospora genome.
278
279 *Changes in H3K9me3-deposition and heterochromatin bundling in* Δcdp-2 *and* Δchap *strains*
280 Given the gain of constitutive heterochromatic acetylation in HCHC mutants, we examined H3K9me3
281 enrichment by ChIP-seq to assess other possible histone PTM differences in permanently silent loci in Δ*cdp-*
282 *2* and Δ*chap* strains. The H3K9me3 ChIP-seq replicates of each strain are reproducible (Figure S18), allowing
283 us to merge the replicates from each strain. Most H3K9me3 enrichment in WT and Δ*cdp-2* strains is similar
284 (Figure 3A). However, several moderate to small-sized heterochromatic regions normally enriched with
285 H3K9me3 in WT are nearly devoid of H3K9me3 in a Δ*cdp-2* strain (Figures 3A, S19A asterisks), while nearby
286 heterochromatic regions still retain H3K9me3; regions that lose H3K9me3 do not gain H3K9ac (Figure
287 S19A). Zooming into two affected regions, we observe background levels of H3K9me3 across the entire locus,
288 indicating read mapping is unaffected and arguing against underlying DNA changes causing H3K9me3 loss
289 (Figure S19A). In contrast, CHAP removal causes subtle H3K9me3 gains in most heterochromatic regions,
290 relative to WT, even with RPKM normalization, (Figure S15A). Average enrichment plots and heatmaps, the
291 latter ordered by region length, show most heterochromatic regions, but not genes, gain H3K9me3
292 enrichment in a Δ*chap* strain (Figure S15D-E). Conversely, while many larger heterochromatic regions have

293 unchanged H3K9me3 with CDP-2 loss, there is a tendency of smaller AT-rich loci to have a near-complete
294 loss of H3K9me3 (Figures 3C, S19B). Boxplots of average signal across scaled, WT-defined heterochromatic
295 regions highlight the lower H3K9me3 signal across all AT-rich regions in a Δ*cdp-2* strain (Figure S19C).
296 Interestingly, borders of heterochromatic regions often have the most pronounced H4K16ac increase and
297 H3K9me3 depletion upon CDP-2 loss (Figure S20A-B). To highlight if the same regions that gain H4K16ac
298 also lose H3K9me3, we k-means clustered the signal of these two marks across heterochromatic regions. K-
299 means cluster heatmaps extending +/-15 kb or +/-2 kb show how individual AT-rich regions gain H4K16ac
300 and lose H3K9me3 in a Δ*cdp-2* strain (Figure S20C-D).

301 We hypothesized that the H3K9me3 loss and H4K16ac gain might affect the genome organization of these
302 formerly heterochromatic regions. To this end, we plotted the Hi-C contact probability changes between WT
303 and Δ*cdp-2* datasets across two regions on LG I and LG III, each of which encompass AT-rich regions losing
304 H3K9me3 in a Δ*cdp-2* strain (Figures 3D, S21). In both instances, H3K9me3-deficient regions strongly gain
305 contacts with other AT rich regions retaining this silencing mark. For example, on LG I, the loss of H3K9me3
306 from (and concomitant gain of H4K16ac in) multiple AT-rich loci caused gains in inter-region contacts, while
307 several nearby regions retaining H3K9me3 are unaffected (Figure 3D, closed arrowheads). On LG III, the
308 contacts between two nearby AT-rich genomic regions are increased when one region loses H3K9me3, while
309 two similarly sized heterochromatic regions have few long-range interaction changes (Figure S21, compare
310 closed and open arrowheads). All told, the loss of CDP-2 impacts histone PTM enrichment, which causes
311 increases in contact probability between AT-rich loci in heterochromatin bundles.

312

313 *Changes in histone PTMs and genome organization in a* Δcdp-2;Δdim-2 *double mutant*

314 To this point, we have shown that the heterochromatic regions of strains individually deleted of HCHC
315 complex members gain acetylation, which alters H3K9me3 deposition and heterochromatin bundling.
316 However, CDP-2 or CHAP removal also alters cytosine methylation levels: centromeres and other large
317 interspersed heterochromatic regions gain $5^{m}C$, while smaller AT-rich loci lose $5^{m}C$ (39, 40). Hypothetically,
318 the extra heterochromatic $5^{m}C$ in an HCHC mutant may confer additional properties to AT-rich loci, meaning
319 $5^{m}C$ gains should be considered when assessing genome organization. In support, a Δ*cdp-2*;Δ*dim-2* strain

320 devoid of the only DNA methyltransferase in Neurospora, has a compromised growth rate relative to single
321 HCHC mutants (40).

322 To understand if an increase in 5^{m}C alters histone PTM deposition following HCHC complex loss, we
323 examined levels of H4K16ac and H3K9me3 in a Δ*cdp-2*;Δ*dim-2* double mutant strain. Our ChIP-seq replicate
324 experiments are qualitatively comparable (Figures S14, S18), allowing us to merge identical, RPKM
325 normalized, ChIP-seq histone PTM replicates. The distribution of H4K16ac in a Δ*cdp-2*;Δ*dim-2* strain mirrors
326 that of Δ*cdp-2*, as both mutant strains gain H4K16ac across all heterochromatic regions, regardless of size,
327 while genic acetylation is minimally altered (Figure 4A-B, S22A). The average heterochromatic H4K16ac
328 signal in a Δ*cdp-2*;Δ*dim-2* strain is slightly reduced compared to Δ*cdp-2* but strongly increased relative to WT
329 H4K16ac levels (Figure S22B). Interestingly, most AT-rich regions in a Δ*cdp-2*;Δ*dim-2* strain strongly gain
330 H3K9me3 when compared to WT and Δ*cdp-2* strains (Figures 4A), as evident in heatmaps of the H3K9me3
331 enrichment across sorted regions (Figures 4C, S22C), or boxplots of the average H3K9me3 deposition across
332 scaled AT-rich regions (Figure S22D). However, the same, typically smaller, AT-rich regions completely lack
333 H3K9me3 in both the Δ*cdp-2* and double mutant strains (Figures 4A, asterisks; 4C). Thus, histone acetylation
334 gains coupled with 5^{m}C loss at AT-rich loci signals for increased H3K9me3 by the DCDC (38).

335 To assess if enhanced heterochromatic acetylation coupled with 5^{m}C loss impacts genome organization,
336 we performed euchromatin-specific (*Dpn*II) *in situ* Hi-C to generally assess genome organization of the Δ*cdp-*
337 *2*;Δ*dim-2* strain. We generated two highly correlated *in situ Dpn*II Hi-C replicates of a Δ*cdp-2*;Δ*dim-2* strain
338 (Figure S23), which we merged into a single *Dpn*II Δ*cdp-2*;Δ*dim-2* Hi-C dataset containing 23.1M valid read
339 pairs (Table S1). The contact frequency heatmap for the Δ*cdp-2*;Δ*dim-2* strain still shows some segregation
340 of heterochromatin from euchromatin, as observed across each individual chromosome (Figure S24) and the
341 entire genome (Figure S25). The KR-corrected whole genome contact probability heatmap also shows
342 centromere bundles independent of telomere clusters typical of the Rabl conformation (Figure S25B).

343 However, comparison of equal numbers of valid read pairs between the Δ*cdp-2*;Δ*dim-2* and WT *Dpn*II Hi-
344 C datasets showed evidence of genome disorder in the double mutant, with heterochromatic regions in Δ*cdp-*
345 *2*;Δ*dim-2* interacting more with surrounding euchromatin. Both raw and KR corrected heatmaps comparing
346 WT and Δ*cdp-2*;Δ*dim-2* contact probabilities show that AT-rich, heterochromatic loci, including the

347 centromere, gain interactions with flanking euchromatic DNA across all LGs (Figure S26), including LG II
348 (Figure 5A). Notably, the increased interactions between heterochromatic regions evident upon CDP-2 loss
349 (e.g., Figures 1B-D) are not apparent in a Δ*cdp-2*;Δ*dim-2* strain. Further, obvious reductions in local and
350 regional euchromatic interactions are observed (Figure 5A). We quantified the intra-chromosomal contact
351 probability changes between the Δ*cdp-2*;Δ*dim-2* and WT datasets among bins enriched for heterochromatic
352 or euchromatic histone PTMs. Few H3K9me3-enriched bins had strongly increased contacts with other
353 heterochromatic bins, but more H3K9me3-marked bins gained contacts with euchromatic bins enriched for
354 SET-2 H3K36me3 or H3K27ac; most contact probability gains occur between euchromatic bins (Figure 5B).
355 Comparison of WT and Δ*cdp-2*;Δ*dim-2* datasets across the whole genome, independent of KR correction,
356 shows increases in inter-chromosomal contact probability between heterochromatin and euchromatin,
357 which depletes local intra-chromosomal contacts (Figure S27). Quantifying the strongly increased inter-
358 chromosomal contacts shows H3K9me3-marked bins gaining interactions with bins enriched with
359 euchromatic SET-2-dependent H3K36me2 and H3K27ac; the number of H3K27ac-enriched bins gaining
360 inter-chromosomal contacts to SET-2-dependent H3K36me2-enriched bins is also increased (Figure 5B). We
361 conclude that the Δ*cdp-2*;Δ*dim-2* heterochromatin bundle is disordered with histone hyperacetylation and
362 $5^{m}C$ depletion.

363 We compared the *Dpn*II Hi-C data of the Δ*cdp-2* single mutant and the Δ*cdp-2*;Δ*dim-2* double mutant to
364 highlight the genome organization changes caused by both hyperacetylation and loss of $5^{m}C$. Across LG II, the
365 Δ*cdp-2*;Δ*dim-2* strain presents with stronger gains in contact frequency between heterochromatin and
366 euchromatin, increases in regional euchromatic contacts across TAD-like structures, and decreased local (on-
367 diagonal) contacts relative to a Δ*cdp-2* strain (Figure 5C); similar changes occur over the entire Neurospora
368 genome and across the other LGs (Figures S28, S29). Closer examination of the regional contact changes
369 between AT-rich loci and euchromatin highlight how loss of both CDP-2 and DIM-2 impacts chromosome
370 conformation. Relative to WT, individual H3K9me3-enriched loci in a Δ*cdp-2*;Δ*dim-2* strain more strongly
371 contact euchromatin, thereby depleting euchromatic clustering; this phenotype is exacerbated when
372 comparing Δ*cdp-2*;Δ*dim-2* and Δ*cdp-2* contact probabilities (Figure 5D). We conclude that heterochromatic
373 hyperacetylation and $5^{m}C$ loss compromises the normal chromosome conformation in Neurospora nuclei.

374

375 **Discussion**

376 In this work, we examined the role of CDP-2 and CHAP, as members of the constitutive heterochromatin-
377 specific histone deacetylase complex HCHC, in modulating histone PTM enrichment and the genome
378 organization of *Neurospora crassa*. Here, heterochromatin hyperacetylation in a Δ*cdp-2* strain causes
379 increased contact probability within heterochromatic loci, as well as between distant intra- and inter-
380 chromosomal heterochromatic regions, while CHAP loss reduces heterochromatin aggregation without
381 strong histone acetylation changes. Neither gene deletion abolished the Rabl chromosome conformation
382 typical of fungal genomes (28), suggesting the overall genome organization can still form despite HCHC loss.
383 Together, our data suggest that CDP-2 and CHAP have distinct functions in the HCHC complex that
384 differentially impact genome organization. Our model (Figure 6) is that CDP-2 recruits the HDA-1
385 deacetylase to properly compact individual heterochromatic regions while CHAP mediates heterochromatic
386 region aggregation at the nuclear periphery after deacetylation. Specifically, the hyperacetylation seen with
387 CDP-2 loss could open chromatin fibers and/or loosen the DNA wrapped about histones in heterochromatic
388 nucleosomes, which would increase heterochromatin accessibility to allow greater contact probability with
389 distant heterochromatic nucleosomes in the silent "B" compartment at the nuclear periphery (14) and
390 indirectly increase the association of euchromatic regions across chromosome arms. One intriguing
391 hypothesis is that the increased chromatin accessibility that occurs from enhanced heterochromatic
392 nucleosome turnover, as observed in HDAC mutants in *S. pombe* and *N. crassa* (78, 79), could amplify the
393 contact probability within and between heterochromatic regions upon CDP-2 loss. Regarding CHAP, this
394 HCHC complex member compacts heterochromatic regions into dense structures and mediates inter-
395 heterochromatic region contacts, possibly through direct AT-rich DNA binding by its AT-hook motifs (39).
396 Since CDP-2 and CHAP recruit HDA-1 to AT-rich loci (39), these proteins most likely act prior to HDA-1,
397 meaning the genome organizational changes we observe reflect inadequate HDA-1 targeting or deficient
398 HCHC complex formation or function. Notably, the loss of the fourth HCHC complex member, HP1, has a
399 genome organization distinct from that of Δ*cdp-2* or Δ*chap* strains, as flanking euchromatin emanating from
400 heterochromatic regions has reduced contact probabilities in WT vs. Δ*hpo* datasets, similar to that of a Δ*dim-*

401 *5* strain lacking H3K9me3 (27), however *in situ* Hi-C could reveal other Δ*hpo*-specific genome organization
402 changes. Thus, HP1 binding to H3K9me3 presumably occurs prior to, or in parallel with, CHAP condensing
403 AT-rich regions; CHAP and HP1 could both act prior to CDP-2 binding HP1 for HDA-1 recruitment (39). This
404 proposed mechanism for Neurospora HCHC activity may be homologous to yeast HDAC complexes. In
405 *Saccharomyces cerevisiae*, Sirtuin-2 (Sir2; a Class III HDAC)-specific deacetylation is required for the binding
406 of the Sir3/Sir4 dimer onto deacetylated histone tails to form silenced superstructures at heterochromatic
407 loci in the budding yeast genome (50, 58, 80, 81). *S. cerevisiae* also employs the HDACs Rpd3 (Class I) and
408 HDA-1 (Class II) for euchromatic deacetylation (58, 82–84); Rpd3 forms two distinct HDAC complexes, the
409 Rpd3L (large) complex targeting promoters and the Rpd3S (small) complex deacetylating gene bodies (84–
410 86). In *Schizosaccharomyces pombe*, the multisubunit HDAC complex SHREC (***S***nf2/***H***dac-containing
411 ***Re***pressor ***C***omplex) is targeted to heterochromatic loci by the HP1-homolog Swi6 for transcriptional gene
412 silencing, although SHREC can localize to euchromatin independent of Swi6 (87–89). The SHREC catalytic
413 subunit Clr3 is homologous to Neurospora HDA-1, and at least three other HDA-1 paralogs and a Rpd3
414 homolog exist in Neurospora (41). Notably, we used the general HDAC inhibitor Trichostatin A (TSA) to
415 examine if all HDACs have roles in genome organization, yet TSA severely compromised WT growth,
416 suggesting HDAC paralogs also influence fungal genome function. Examination of other HDACs in
417 Neurospora by Hi-C or ChIP-seq could elucidate how HDAC paralogs impact chromosome conformation or
418 histone PTM deposition.

419 As previously shown by ChIP qPCR, multiple histone lysines become hyperacetylated upon loss of HDA-
420 1 and CDP-2; the extent of hyperacetylation depends on both the heterochromatic region assessed and which
421 HCHC member was deleted (40). This published ChIP qPCR data, as well as our genome-wide ChIP-seq
422 acetylation data, hints at the HCHC complex having preferential deacetylation activity for certain lysine
423 residues in histones. Specifically, our ChIP-seq data shows heterochromatin in a Δ*cdp-2* strain becoming
424 hyperacetylated at H4K16 but minimally changed at H3K9, while heterochromatic H4K16ac enrichment is
425 minimally altered in a Δ*chap* strain; perhaps HP1 or CDP-2, both of which can bind to H3K9me3 (40, 90, 91),
426 can compensate for CHAP loss and still allow for HDA-1 deacetylation. The unchanged H3K9ac enrichment
427 in a Δ*cdp-2* strain may reflect DCDC-dependent (38) tri-methylation of H3K9, given the mutually exclusive

428 deposition of either acetylation or trimethylation on H3K9 (92, 93). Currently, it is unknown if H4K16ac is
429 globally enriched in Δ*hpo* heterochromatin, or whether other histone acetyl marks have altered enrichment
430 in HCHC mutants. Future ChIP-seq experiments on other acetylated histone lysine residues in Δ*cdp-2,* Δ*chap*,
431 Δ*hpo*, or Δ*hda-1* strains should uncover genome-wide changes to acetylation patterns for understanding the
432 lysine specificity of the HCHC complex.

433 Interestingly, while Δ*cdp-2* or Δ*chap* strains gain heterochromatin-specific H4K16ac relative to WT, these
434 mutant strains display no change in euchromatic acetylation, suggesting the HCHC complex specifically
435 deacetylates heterochromatic histones. Since both the class II HDAC HDA-1 in Neurospora and the class III
436 HDACs Hst2p and Sir2 in *S. cerevisiae* are both known to deacetylate H4K16 (63, 81), yet they share little
437 primary structure similarity, it is possible that different HDACs can deacetylate identical histone lysines but
438 the targeting mechanism of each HDAC complex determines which genomic loci are deacetylated. Given that
439 HDA-1 is targeted to heterochromatic nucleosomes by CHAP binding AT-rich DNA and HP1/CDP-2 binding
440 H3K9me3 (39, 40), these factors would render the HCHC complex as a heterochromatin-specific HDAC. This
441 explains the copious HCHC mutants recovered in a selection for strains with compromised heterochromatin
442 silencing (94); it is possible the HCHC complex is the only heterochromatin specific HDAC in Neurospora.
443 Our data also suggest that unknown HAT(s) specifically acetylate heterochromatic H4K16 – which is only
444 seen with compromised HCHC HDAC activity – given that euchromatic acetylation is minimally altered in
445 HCHC mutants. Presumably, Neurospora could repress HCHC expression or activity to hyperacetylate
446 heterochromatin for altering genome organization at certain developmental or cell cycle stages, including S
447 phase in which a more open chromosome conformation exists in fission yeast (95). Conversely, Neurospora
448 may increase expression of the HCHC complex and/or other HDACs to hypoacetylate mitotic chromatin for
449 segregating condensed chromosomes to daughter cells; rapid HDAC repression would allow chromatin to be
450 rapidly acetylated following cytokinesis, as previously observed (63, 64). It is noteworthy that the increased
451 contact probability occurring between hyperacetylated, yet distant, heterochromatic regions in Δ*cdp-2* nuclei
452 is analogous to the clustering of hyperacetylated chromatin in BRD4-NUT expressing oncogenic cells (68).
453 Together, changes in acetylation patterns that alter chromatin accessibility could represent a simple
454 mechanism that eukaryotes employ to differentially organize their genomes.

455 Curiously, smaller AT-rich regions in a Δ*cdp-2* strain lose H3K9me3 yet this mark remains unchanged at
456 larger heterochromatic loci, while a Δ*chap* strain has modest H3K9me3 gains at most AT-rich regions,
457 highlighting the differential effects of HCHC mutants on heterochromatic histone PTMs. Apart from size,
458 other possible causes of locus-specific H3K9me3 loss in CDP-2 deficient strains include compromised
459 subnuclear positioning, reduced pairing with other AT-rich regions (96), or unrecognized transposon relict
460 motifs in the underlying DNA (97). In contrast, the H3K9me3 gain in a Δ*chap* strain may result from increased
461 DCDC levels or activity, which would promote further AT-rich region compaction through additional HP1
462 binding sites. Similar increases in the DCDC subunits DIM-7 and DIM-9 occur in a *dim-3* strain to possibly
463 rescue reduced H3K9me3 levels (98). Our data suggest that WT heterochromatic nucleosomes are not
464 saturated with H3K9me3, given that greater levels of H3K9me3 are possible in some mutant HCHC strains.
465 Notably, changes in H3K9me3 deposition can impact the enrichment of the H3K27me2/3 histone PTM that
466 marks facultative heterochromatin, for in DCDC deficient strains, H3K27me2/3 relocates to AT-rich genomic
467 loci (99, 100). While ChIP qPCR showed no H3K27me2/3 change at a few loci in HCHC deletion strains (99),
468 examination of the global enrichment of H3K27me2/3 in HCHC deficient backgrounds would be prudent,
469 given the changes in H3K9me3 deposition reported here.
470 Changes in H3K9me3 are most apparent in a Δ*cdp-2*;Δ*dim-2* double mutant, where most heterochromatic
471 regions gain considerable H3K9me3 enrichment, although smaller AT-rich regions similarly lose H3K9me3
472 as a single Δ*cdp-2* mutant; all AT-rich loci gain H4K16ac in both strains. These results suggest the loss of $5^{m}C$
473 signals for the H3K9me3 increase but does not affect histone acetylation. Importantly, the genome
474 organization of the double mutant is disordered, as AT-rich heterochromatic regions amalgamate with
475 euchromatin despite greater H3K9me3 deposition (and presumably HP1 binding). These results may explain
476 the severe growth defect of Δ*cdp-2*;Δ*dim-2* strains (40), as improper positioning of AT-rich regions into the
477 nucleus center may cause aberrant transcription of repetitive DNA or limit normal genic transcription, the
478 latter being particularly deleterious given how heterochromatic-euchromatic contacts mediate proper gene
479 expression in filamentous fungi (16, 101). Perhaps the increased H3K9me3 enrichment in the Δ*cdp-2*;Δ*dim-*
480 *2* strain is a "last resort" by the fungus to repress AT-rich region transcription in the nucleus center, where
481 increased H3K9me3 and HP1 compaction could minimize RNA Pol II recruitment to this mislocalized

482 chromatin. A crucial, unanswered question is: "how is H3K9me3 enrichment increased?" We speculate that
483 reduced AT-rich region compaction, observed in both Δ*chap* and Δ*cdp-2*;Δ*dim-2* strains, signals for increased
484 H3K9me3 deposition. Consistent with this hypothesis, intergenic region nucleosomal disorder causes subtle
485 increases in H3K9me3 in Neurospora *dim-1* strains (102), but this remains to be seen in HCHC mutants.

486 Importantly, our double mutant Hi-C results suggest that cytosine methylation maintains chromatin
487 compartmentalization by segregating hyperacetylated heterochromatin from euchromatin. Specifically, only
488 in strains devoid of both CDP-2 and DIM-2 are AT-rich regions more apt to contact euchromatin. However,
489 this change only moderately affects the global genome topology, since the Rabl chromosome conformation
490 is still maintained, although the weak chromosome territories typically seen in Neurospora are diminished
491 in Δ*cdp-2*;Δ*dim-2* nuclei. These results suggest heterochromatin can cluster, as in WT, but unlike the situation
492 in a Δ*cdp-2* strain, the inter-heterochromatic contact gains are abrogated by $5^{m}C$ loss. We speculate the
493 additional methyl groups on AT-rich DNA in a Δ*cdp-2* strain allow heterochromatic regions to remain
494 associated with the nuclear periphery, either by active recruitment by a methyl-DNA binding protein (MRBP-
495 1) (103, 104) or passively by Liquid-Liquid Phase Separation (105). The identity of MRBP-1 in Neurospora
496 is unknown, as Neurospora does not encode a protein with a strong MBD domain homologous to human
497 MeCP-2, but perhaps DIM-10, which compromises heterochromatin silencing but not $5^{m}C$ deposition or
498 H3K9me3 enrichment (94), could bind methylated DNA in Neurospora. Regardless, our results suggest a new
499 role for $5^{m}C$ in maintaining chromatin compartmentalization when heterochromatin is compromised,
500 thereby safeguarding genome organization and function. Future experiments should discern if $5^{m}C$ has a
501 similar role in maintaining genome topology in fungal pathogens or higher eukaryotes.

502

503 **Materials and Methods**

504 The strains used for all experiments, the abbreviated Hi-C and ChIP-seq protocols, and the bioinformatic
505 methods are found in the online Materials and Methods, provided in Supplementary File 1. *In situ* Hi-C was
506 performed as in (16), using the program hicExplorer (73) to process mapped reads for building the contact
507 matrices, which were used for all downstream analyses and image generation. ChIP-seq performed as in (32,
508 102), with minor modifications. The complete *in situ* Hi-C protocol is provided in Supplementary File 2, while

509 the ChIP-seq protocol is found in Supplementary File 3.

510

511 **Data availability**

512 All *Neurospora crassa* strains are available upon request. The *in situ* Hi-C and ChIP-seq high-throughput
513 sequencing data are available in the NCBI GEO superseries accession number GSE232935, which includes
514 the ChIP-seq data accession number GSE232933 and the Hi-C data accession number GSE232934.

515

516 **Acknowledgements**

517 The authors wish to thank UCCS Andrew Reckard, Sara Rodriguez, Yulia Shtanko, Victoria Toscano, and
518 Farh Kaddar (UCCS) for assistance with library generation, preliminary data analysis, or critical reading of
519 the manuscript, Doug Turnbull and Jeff Bishop (University of Oregon Genomics and Cell Characterization
520 Core Facility) for Illumina library sequencing service, and all Klocko lab members and colleagues of the UCCS
521 Department of Chemistry & Biochemistry for helpful comments and discussions. Funding was provided by
522 start-up funds from the UCCS College of Letters, Arts, and Sciences and an Academic Research Enhancement
523 Award (AREA) grant from the National Institutes of Health (1R15GM140396-01) to A.D.K.

524

525 **References**

526 1. T. Cremer, C. Cremer, Chromosome territories, nuclear architecture and gene regulation in mammalian
527 cells. *Nat Rev Genet* **2**, 292–301 (2001).

528 2. T. Misteli, Beyond the Sequence: Cellular Organization of Genome Function. *Cell* **128**, 787–800 (2007).

529 3. J. Dekker, Gene Regulation in the Third Dimension. *Science* **319**, 1793–1794 (2008).

530 4. T. Sexton, G. Cavalli, The Role of Chromosome Domains in Shaping the Functional Genome. *Cell* **160**, 1049–
531 1059 (2015).

532 5. B. Bonev, G. Cavalli, Organization and function of the 3D genome. *Nat Rev Genet* **17**, 661–678 (2016).

533 6. M. Falk, *et al.*, Heterochromatin drives compartmentalization of inverted and conventional nuclei. *Nature*
534 **570**, 395–399 (2019).

535 7. A. J. Shatkin, E. L. Tatum, Electron Microscopy of *Neurospora crassa* Mycelia. *J Biophys Biochem Cytol* **6**,
536 423–426 (1959).

537 8. A. Buchwalter, J. M. Kaneshiro, M. W. Hetzer, Coaching from the sidelines: the nuclear periphery in genome
538 regulation. *Nat Rev Genet* **20**, 39–50 (2019).

539 9. S. Schoenfelder, *et al.*, Preferential associations between co-regulated genes reveal a transcriptional
540 interactome in erythroid cells. *Nat Genet* **42**, 53–61 (2010).

541 10. E. E. M. Furlong, M. Levine, Developmental enhancers and chromosome topology. *Science* **361**, 1341–
542 1345 (2018).

543 11. P. A. Northcott, *et al.*, Enhancer hijacking activates GFI1 family oncogenes in medulloblastoma. *Nature*
544 **511**, 428–34 (2014).

545 12. W. A. Flavahan, *et al.*, Insulator dysfunction and oncogene activation in IDH mutant gliomas. *Nature* **529**,
546 110–114 (2016).

547 13. Z. Xu, *et al.*, Structural variants drive context-dependent oncogene activation in cancer. *Nature*, 1–9
548 (2022).

549 14. E. Lieberman-Aiden, *et al.*, Comprehensive Mapping of Long-Range Interactions Reveals Folding
550 Principles of the Human Genome. *Science* **326**, 289–293 (2009).

551 15. S. S. P. Rao, *et al.*, A 3D Map of the Human Genome at Kilobase Resolution Reveals Principles of Chromatin
552 Looping. *Cell* **159**, 1665–1680 (2014).

553 16. S. Rodriguez, *et al.*, The genome organization of Neurospora crassa at high resolution uncovers principles
554 of fungal chromosome topology. *G3 Genes Genomes Genetics* **12**, jkac053 (2022).

555 17. K. Luger, A. W. Mäder, R. K. Richmond, D. F. Sargent, T. J. Richmond, Crystal structure of the nucleosome
556 core particle at 2.8 Å resolution. *Nature* **389**, 251–260 (1997).

557 18. E. I. Campos, D. Reinberg, Histones: Annotating Chromatin. *Annu Rev Genet* **43**, 559–599 (2009).

558 19. J. R. Dixon, *et al.*, Topological Domains in Mammalian Genomes Identified by Analysis of Chromatin
559 Interactions. *Nature* **485**, 376–380 (2012).

560 20. J. Dekker, E. Heard, Structural and functional diversity of Topologically Associating Domains. *FEBS Lett*
561 **589**, 2877–2884 (2015).

562 21. A. S. Hansen, C. Cattoglio, X. Darzacq, R. Tjian, Recent evidence that TADs and chromatin loops are
563 dynamic structures. *Nucleus* **9**, 20–32 (2018).

564 22. M. Imakaev, *et al.*, Iterative correction of Hi-C data reveals hallmarks of chromosome organization. *Nat*
565 *Methods* **9**, 999–1003 (2012).

566 23. T. Cremer, M. Cremer, Chromosome territories. *CSH Perspect Biol* **2**, a003889 (2010).

567 24. C. Hoencamp, *et al.*, 3D genomics across the tree of life reveals condensin II as a determinant of
568 architecture type. *Science* **372**, 984–989 (2021).

569 25. M. R. Speicher, N. P. Carter, The new cytogenetics: blurring the boundaries with molecular biology. *Nat*
570 *Rev Genet* **6**, 782–792 (2005).

571 26. A. D. Klocko, *et al.*, Normal chromosome conformation depends on subtelomeric facultative
572 heterochromatin in *Neurospora crassa*. *Proc Natl Acad Sci* **113**, 15048–15053 (2016).

573 27. J. M. Galazka, *et al.*, Neurospora chromosomes are organized by blocks of importin alpha-dependent
574 heterochromatin that are largely independent of H3K9me3. *Genome Res* **26**, 1069–1080 (2016).

575 28. D. E. Torres, A. T. Reckard, A. D. Klocko, M. F. Seidl, Nuclear genome organization in fungi: From gene
576 folding to Rabl chromosomes. *FEMS Microbiol Rev* **43**, fuad021 (2023).

577 29. J. E. Galagan, *et al.*, The genome sequence of the filamentous fungus *Neurospora crassa*. *Nature* **422**, 859–
578 868 (2003).

579 30. Z. A. Lewis, *et al.*, Relics of repeat-induced point mutation direct heterochromatin formation in
580 *Neurospora crassa*. *Genome Res* **19**, 427–437 (2009).

581 31. M. R. Rountree, E. U. Selker, DNA methylation and the formation of heterochromatin in *Neurospora crassa*.
582 *Heredity* **105**, 38–44 (2010).

583 32. K. Jamieson, M. R. Rountree, Z. A. Lewis, J. E. Stajich, E. U. Selker, Regional control of histone H3 lysine 27
584 methylation in Neurospora. *Proc Natl Acad Sci* **110**, 6027–6032 (2013).

585 33. V. T. Bicocca, T. Ormsby, K. K. Adhvaryu, S. Honda, E. U. Selker, ASH1-catalyzed H3K36 methylation drives
586 gene repression and marks H3K27me2/3-competent chromatin. *Elife* **7**, e41497 (2018).

587 34. H. Tamaru, *et al.*, Trimethylated lysine 9 of histone H3 is a mark for DNA methylation in *Neurospora*
588 *crassa*. *Nat Genet* **34**, 75–79 (2003).

589 35. E. U. Selker, J. N. Stevens, DNA methylation at asymmetric sites is associated with numerous transition
590 mutations. *Proc Natl Acad Sci* **82**, 8114–8118 (1985).

591 36. E. T. Wiles, E. U. Selker, H3K27 methylation: a promiscuous repressive chromatin mark. *Curr Opin Genet*
592 *Dev* **43**, 31–37 (2017).

593 37. E. U. Selker, *et al.*, The methylated component of the *Neurospora crassa* genome. *Nature* **422**, 893–897
594 (2003).

595 38. Z. A. Lewis, *et al.*, DNA Methylation and Normal Chromosome Behavior in Neurospora Depend on Five
596 Components of a Histone Methyltransferase Complex, DCDC. *PLoS Genet* **6**, e1001196 (2010).

597 39. S. Honda, *et al.*, Dual chromatin recognition by the histone deacetylase complex HCHC is required for
598 proper DNA methylation in *Neurospora crassa*. *Proc Natl Acad Sci* **113**, E6135–E6144 (2016).

599 40. S. Honda, *et al.*, Heterochromatin protein 1 forms distinct complexes to direct histone deacetylation and
600 DNA methylation. *Nat Struct Mol Biol* **19**, 471–477 (2012).

601 41. K. M. Smith, *et al.*, H2B- and H3-Specific Histone Deacetylases Are Required for DNA Methylation in
602 *Neurospora crassa*. *Genetics* **186**, 1207–1216 (2010).

603 42. H. Foss, C. Roberts, K. Claeys, E. Selker, Abnormal chromosome behavior in Neurospora mutants defective
604 in DNA methylation. *Science* **262**, 1737–1741 (1993).

605 43. T. Mizuguchi, *et al.*, Cohesin-dependent globules and heterochromatin shape 3D genome architecture in
606 *S. pombe*. *Nature* **516**, 432–435 (2014).

607 44. S. I. S. Grewal, S. Jia, Heterochromatin revisited. *Nat Rev Genetics* **8**, 35–46 (2007).

608 45. A. J. Courtney, A. R. Ferraro, A. D. Klocko, Z. A. Lewis, "Chromatin Structure and Function in *Neurospora*
609 *crassa*." in *The Mycota, A Comprehensive Treatise on Fungi as Experimental Systems, Third Edition for Basic*
610 *and Applied Research, Genetics and Biotechnology*, J. P. Benz, K. Schipper, Eds. (Springer Nature Switzerland
611 AG, 2020), pp. 3–24.

612 46. T. Jenuwein, C. D. Allis, Translating the Histone Code. *Science* **293**, 1074–1080 (2001).

613 47. F. Zenk, *et al.*, HP1 drives *de novo* 3D genome reorganization in early Drosophila embryos. *Nature* **593**,
614 289–293 (2021).

615 48. A. Eberharter, P. B. Becker, Histone acetylation: a switch between repressive and permissive chromatin.
616 *EMBO Rep* **3**, 224–229 (2002).

617 49. Y.-J. C. Chen, E. Koutelou, S. Y. R. Dent, Now open: Evolving insights to the roles of lysine acetylation in
618 chromatin organization and function. *Mol Cell* **82**, 716–727 (2022).

619 50. D. M. Thurtle, J. Rine, The molecular topography of silenced chromatin in *Saccharomyces cerevisiae*. *Gene*
620 *Dev* **28**, 245–258 (2014).

621 51. B. J. E. Martin, *et al.*, Transcription shapes genome-wide histone acetylation patterns. *Nat Commun* **12**,
622 210 (2021).

623 52. J. N. McKnight, J. W. Boerma, L. L. Breeden, T. Tsukiyama, Global Promoter Targeting of a Conserved Lysine
624 Deacetylase for Transcriptional Shutoff during Quiescence Entry. *Mol Cell* **59**, 732–743 (2015).

625 53. A. R. Ferraro, *et al.*, Chromatin accessibility profiling in *Neurospora crassa* reveals molecular features
626 associated with accessible and inaccessible chromatin. *BMC Genomics* **22**, 459 (2021).

627 54. T. Conrad, F. M. G. Cavalli, J. M. Vaquerizas, N. M. Luscombe, A. Akhtar, Drosophila Dosage Compensation
628 Involves Enhanced Pol II Recruitment to Male X-Linked Promoters. *Science* **337**, 742–746 (2012).

629 55. S. Fox, *et al.*, Hyperacetylated chromatin domains mark cell type-specific genes and suggest distinct
630 modes of enhancer function. *Nat Commun* **11**, 4544 (2020).

631 56. I. Dunham, *et al.*, An integrated encyclopedia of DNA elements in the human genome. *Nature* **489**, 57–74
632 (2012).

633 57. D. U. Gorkin, *et al.*, An atlas of dynamic chromatin landscapes in mouse fetal development. *Nature* **583**,
634 744–751 (2020).

635 58. E. Seto, M. Yoshida, Erasers of Histone Acetylation: The Histone Deacetylase Enzymes. *CSH Perspect Biol*
636 **6**, a018713 (2014).

637 59. A. J. Rubin, *et al.*, Lineage-specific dynamic and pre-established enhancer–promoter contacts cooperate
638 in terminal differentiation. *Nat Genet* **49**, 1522–1528 (2017).

639 60. R. Siersbæk, *et al.*, Dynamic Rewiring of Promoter-Anchored Chromatin Loops during Adipocyte
640 Differentiation. *Mol Cell* **66**, 420-435.e5 (2017).

641 61. M. W. G. Schneider, *et al.*, A mitotic chromatin phase transition prevents perforation by microtubules.
642 *Nature* **609**, 183–190 (2022).

643 62. A. Zhiteneva, *et al.*, Mitotic post-translational modifications of histones promote chromatin compaction
644 *in vitro*. *Open Biol* **7**, 170076 (2017).

645 63. B. J. Wilkins, *et al.*, A Cascade of Histone Modifications Induces Chromatin Condensation in Mitosis. *Science*
646 **343**, 77–80 (2014).

647 64. M. J. Kruhlak, *et al.*, Regulation of Global Acetylation in Mitosis through Loss of Histone Acetyltransferases
648 and Deacetylases from Chromatin. *J Biol Chem* **276**, 38307–38319 (2001).

649 65. D. Cimini, M. Mattiuzzo, L. Torosantucci, F. Degrassi, Histone Hyperacetylation in Mitosis Prevents Sister
650 Chromatid Separation and Produces Chromosome Segregation Defects. *Mol Biol Cell* **14**, 3821–3833 (2003).

651 66. B. Pelham-Webb, *et al.*, H3K27ac bookmarking promotes rapid post-mitotic activation of the pluripotent
652 stem cell program without impacting 3D chromatin reorganization. *Mol Cell* **81**, 1732-1748.e8 (2021).

653 67. H. Kang, *et al.*, Dynamic regulation of histone modifications and long-range chromosomal interactions
654 during postmitotic transcriptional reactivation. *Gene Dev* **34**, 913–930 (2020).

655 68. C. D. Rosencrance, *et al.*, Chromatin Hyperacetylation Impacts Chromosome Folding by Forming a Nuclear
656 Subcompartment. *Mol Cell* **78**, 112-126.e12 (2020).

657 69. B. A. Gibson, *et al.*, Organization of Chromatin by Intrinsic and Regulated Phase Separation. *Cell* **179**, 470-
658 484.e21 (2019).

659 70. E. Martegani, M. Levi, F. Trezzi, L. Alberghina, Nuclear division cycle in *Neurospora crassa* hyphae under
660 different growth conditions. *J. Bacteriol.* **142**, 268–275 (1980).

661 71. L. Alberghina, E. Sturani, Control of growth and of the nuclear division cycle in *Neurospora crassa*.
662 *Microbiol. Rev.* **45**, 99–122 (1981).

663 72. P. A. Knight, D. Ruiz, A fast algorithm for matrix balancing. *Ima J Numer Anal* **33**, 1029–1047 (2013).

664 73. F. Ramírez, *et al.*, High-resolution TADs reveal DNA sequences underlying genome organization in flies.
665 *Nat Commun* **9**, 189 (2018).

666 74. J. T. Robinson, *et al.*, Integrative genomics viewer. *Nat Biotechnol* **29**, 24–6 (2011).

667 75. N. Bonhoure, *et al.*, Quantifying ChIP-seq data: a spiking method providing an internal reference for
668 sample-to-sample normalization. *Genome Res* **24**, 1157–68 (2014).

669 76. B. Hu, *et al.*, Biological chromodynamics: a general method for measuring protein occupancy across the
670 genome by calibrating ChIP-seq. *Nucleic Acids Res* **43**, gkv670 (2015).

671 77. D. A. Orlando, *et al.*, Quantitative ChIP-Seq Normalization Reveals Global Modulation of the Epigenome.
672 *Cell Reports* **9**, 1163–1170 (2014).

673 78. O. Aygün, S. Mehta, S. I. S. Grewal, HDAC-mediated suppression of histone turnover promotes epigenetic
674 stability of heterochromatin. *Nat Struct Mol Biol* **20**, 547–554 (2013).

675 79. W. K. Storck, S. Z. Abdulla, M. R. Rountree, V. T. Bicocca, E. U. Selker, A Light-Inducible Strain for Genome-
676 Wide Histone Turnover Profiling in *Neurospora crassa*. *Genetics* **215**, 569–578 (2020).

677 80. D. Moazed, A. Kistler, A. Axelrod, J. Rine, A. D. Johnson, Silent information regulator protein complexes in
678 *Saccharomyces cerevisiae*: A SIR2/SIR4 complex and evidence for a regulatory domain in SIR4 that inhibits
679 its interaction with SIR3. *Proc Natl Acad Sci* **94**, 2186–2191 (1997).

680 81. S. Imai, C. M. Armstrong, M. Kaeberlein, L. Guarente, Transcriptional silencing and longevity protein Sir2
681 is an NAD-dependent histone deacetylase. *Nature* **403**, 795–800 (2000).

682 82. J. Wu, A. A. Carmen, R. Kobayashi, N. Suka, M. Grunstein, HDA2 and HDA3 are related proteins that interact
683 with and are essential for the activity of the yeast histone deacetylase HDA1. *Proc Natl Acad Sci* **98**, 4391–
684 4396 (2001).

685 83. S. E. Rundlett, *et al.*, HDA1 and RPD3 are members of distinct yeast histone deacetylase complexes that
686 regulate silencing and transcription. *Proc Natl Acad Sci* **93**, 14503–14508 (1996).

687 84. M. J. Carrozza, *et al.*, Histone H3 Methylation by Set2 Directs Deacetylation of Coding Regions by Rpd3S
688 to Suppress Spurious Intragenic Transcription. *Cell* **123**, 581–592 (2005).

689 85. Z. Guo, *et al.*, Structure of a SIN3–HDAC complex from budding yeast. *Nat Struct Mol Biol*, 1–8 (2023).

690 86. D. Kadosh, K. Struhl, Repression by Ume6 Involves Recruitment of a Complex Containing Sin3
691 Corepressor and Rpd3 Histone Deacetylase to Target Promoters. *Cell* **89**, 365–371 (1997).

692 87. T. Sugiyama, *et al.*, SHREC, an Effector Complex for Heterochromatic Transcriptional Silencing. *Cell* **128**,
693 491–504 (2007).

694 88. G. Job, *et al.*, SHREC Silences Heterochromatin via Distinct Remodeling and Deacetylation Modules. *Mol*
695 *Cell* **62**, 207–221 (2016).

696 89. T. Yamada, W. Fischle, T. Sugiyama, C. D. Allis, S. I. S. Grewal, The Nucleation and Maintenance of
697 Heterochromatin by a Histone Deacetylase in Fission Yeast. *Mol Cell* **20**, 173–185 (2005).

698 90. M. Freitag, P. C. Hickey, T. K. Khlafallah, N. D. Read, E. U. Selker, HP1 Is Essential for DNA Methylation in
699 Neurospora. *Mol Cell* **13**, 427–434 (2004).

700 91. S. A. Jacobs, S. Khorasanizadeh, Structure of HP1 Chromodomain Bound to a Lysine 9-Methylated Histone
701 H3 Tail. *Science* **295**, 2080–2083 (2002).

702 92. A. J. Bannister, T. Kouzarides, Regulation of chromatin by histone modifications. *Cell Res* **21**, 381–395
703 (2011).

704 93. T. Zhang, S. Cooper, N. Brockdorff, The interplay of histone modifications – writers that read. *EMBO Rep*
705 **16**, 1467–1481 (2015).

706 94. A. D. Klocko, *et al.*, Selection and Characterization of Mutants Defective in DNA Methylation in *Neurospora*
707 *crassa*. *Genetics* **216**, genetics.303471.2020 (2020).

708 95. H. Tanizawa, K.-D. Kim, O. Iwasaki, K. Noma, Architectural alterations of the fission yeast genome during
709 the cell cycle. *Nat Struct Mol Biol* **24**, 965–976 (2017).

710 96. N. Rhoades, *et al.*, Recombination-independent recognition of DNA homology for meiotic silencing in
711 *Neurospora crassa*. *Proc Natl Acad Sci* **118**, e2108664118 (2021).

712 97. D. Nguyen, *et al.*, Transposon- and Genome Dynamics in the Fungal Genus Neurospora: Insights from
713 Nearly Gapless Genome Assemblies. *Fungal Genet Rep* **66** (2022).

714 98. A. D. Klocko, *et al.*, Neurospora Importin α Is Required for Normal Heterochromatic Formation and DNA
715 Methylation. *PLoS Genet* **11**, e1005083 (2015).

716 99. K. Jamieson, *et al.*, Loss of HP1 causes depletion of H3K27me3 from facultative heterochromatin and gain
717 of H3K27me2 at constitutive heterochromatin. *Genome Res* **26**, 97–107 (2016).

718 100. E. Y. Basenko, *et al.*, Genome-wide redistribution of H3K27me3 is linked to genotoxic stress and
719 defective growth. *Proc Natl Acad Sci* **112**, E6339–E6348 (2015).

720 101. H. M. Kramer, D. E. Cook, G. C. M. van den Berg, M. F. Seidl, B. P. H. J. Thomma, Three putative DNA
721 methyltransferases of *Verticillium dahliae* differentially contribute to DNA methylation that is dispensable
722 for growth, development and virulence. *Epigenet Chromatin* **14**, 21 (2021).

723 102. A. D. Klocko, *et al.*, Nucleosome Positioning by an Evolutionarily Conserved Chromatin Remodeler
724 Prevents Aberrant DNA Methylation in Neurospora. *Genetics* **211**, 563–578 (2019).

725 103. R. Meehan, J. D. Lewis, A. P. Bird, Characterization of MeCP2, a vertebrate DNA binding protein with
726 affinity for methylated DNA. *Nucleic Acids Res* **20**, 5085–5092 (1992).

727 104. E. U. Selker, *et al.*, Induction and maintenance of nonsymmetrical DNA methylation in Neurospora. *Proc*
728 *Natl Acad Sci* **99**, 16485–16490 (2002).

729 105. A. R. Strom, *et al.*, Phase separation drives heterochromatin domain formation. *Nature* **547**, 241–245
730 (2017).

731

732 **Figure Legends**

733 ***Figure 1. Genome organization changes across a single chromosome in* Neurospora crassa Δcdp-2 *and***
734 **Δchap *strains.*** (A-B) Heatmap of contact probabilities of 20 kb bins across LG II of (A) wild type (WT)
735 *Neurospora crassa* (16) or (B) Δ*cdp-2* strains. Raw read counts of heterochromatin-specific *Mse*I Hi-C (above
736 diagonal) and Knight Ruiz corrected (72, 73) read counts of euchromatin-specific *Dpn*II Hi-C (below
737 diagonal) are presented in heatmaps here and throughout this work unless otherwise indicated. Bin numbers
738 (vertical axis) and genomic distance, in Megabases (Mb), (horizontal axis) are indicated. The scale bar shows
739 the $\log_{10}$ numbers of valid Hi-C contacts per bin. Integrative Genomics Viewer (IGV) (74) images of WT CenH3

740 (red; centromeres) and/or H3K9me3 (green; heterochromatic regions) ChIP-seq tracks are shown above
741 and left. Solid arrowheads in B. show increased inter-heterochromatic contacts; open arrowheads show
742 decreased heterochromatic-euchromatic contacts. (C) The fold change in contact strength ($\log_2$ scale) in a
743 Δ*cdp-2* strain relative to a normalized WT strain of *Mse*I *in situ* Hi-C (above diagonal) or *Dpn*II *in situ* Hi-C
744 (below diagonal) datasets; purple line indicates the region in D. The open arrowhead shows a
745 heterochromatic region gaining internal contacts at the expense of euchromatic contacts. (D) Heatmap of
746 contact probability changes between heterochromatic regions (green) and the LG II centromere in Δ*cdp-2 vs.*
747 WT comparison heatmaps at 10 kb resolution. (E) Quantification of strongly increased ($\log_2 \geq 2.0$), intra-
748 chromosomal contacts in Δ*cdp-2* or Δ*chap* datasets, relative to normalized WT datasets, between bins
749 enriched for select histone PTMs (see Supplemental Materials and Methods). For these graphs, each bar
750 shows the total number of contacts that are strongly ($\log_2 \geq 2.0$) increased. Numbers of contacts originating
751 from bins enriched with the first histone PTM and end in a bin enriched for the second histone PTM are
752 indicated by non-gray colors, while the gray portion of the bar shows contacts originating from the first
753 enriched histone PTM bin but terminating in a non-enriched bin. The percentage of total contacts enriched
754 for both histone PTMs is indicated above. (F) Contact probability heatmap of a Δ*chap* dataset, as in A. (G)
755 Heatmap of contact probability changes between Δ*chap* and WT datasets, as in C.
756
757 ***Figure 2.* Δcdp-2 *and* Δchap *strains alter the inter-chromosomal genome organization.*** (A-B) The $\log_2$
758 contact strength change of (A) Δ*cdp-2* or (B) Δ*chap* datasets, relative to normalized WT dataset between LG
759 II and LG III within *Mse*I *in situ* Hi-C datasets, displayed similarly as Figure 1C. (C) Quantification of strongly
760 increased, inter-chromosomal contacts in Δ*cdp-2* or Δ*chap* datasets relative to a WT dataset, as in Figure 1E.
761
762 ***Figure 3. CDP-2 deletion increases heterochromatic H4K16ac while smaller heterochromatic regions***
763 ***lose H3K9me3.*** (A) IGV images of H3K9me3, H4K16ac, and H3K9ac ChIP-seq enrichment tracks from WT
764 and Δ*cdp-2* strains across LG II (top) and the LG II right arm (bottom). SET-2-specific H3K27ac (from a
765 Δ*ash1*^{Y833F} strain (33)) shows euchromatin. Arrowheads highlight heterochromatic regions gaining H4K16ac
766 enrichment, while asterisks show AT-rich regions losing H3K9me3 in Δ*cdp-2*. (B-C) Average enrichment

767 heatmaps of the (B) H4K16ac or (C) H3K9me3 enrichment in WT and Δ*cdp-2* strains centered over WT-
768 defined constitutive heterochromatic regions (16), extending +/- 15 kb from heterochromatic region centers
769 (top) or +/- 2 kb of the smallest regions (bottom; indicated by the purple line in +/-15 kb plots). (D)
770 Heatmaps of contact probability change between Δ*cdp-2* and WT *Mse*I datasets of a small region of LG I.
771 H3K9me3 and/or H4K16ac ChIP-seq track images shown with each heatmap. Asterisks indicate regions
772 losing H3K9me3, pink arrowheads show regions gaining H4K16ac in a Δ*cdp-2* strain, and black arrowheads
773 highlight gains in inter-heterochromatic region contacts in a Δ*cdp-2* strain.
774
775 ***Figure 4. Constitutive heterochromatic regions gain H4K16ac and H3K9me3 enrichment upon CDP-2***
776 ***and DIM-2 loss.*** (A) IGV images of H3K9me3 and H4K16ac ChIP-seq enrichment tracks of WT, Δ*cdp-2*, and
777 Δ*cdp-2;*Δ*dim-2* strains, as in Figure 3A. Asterisks indicate AT-rich regions losing H3K9me3 enrichment in
778 both Δ*cdp-2* and Δ*cdp-2;*Δ*dim-2* strains. (B-C) Average enrichment heatmaps of (B) H4K16ac or (C) H3K9me3
779 levels in WT, Δ*cdp-2*, and Δ*cdp-2;*Δ*dim-2* strains centered over WT-defined constitutive heterochromatic
780 regions, as in Figures 3B-C.
781
782 ***Figure 5. A* Δcdp-2;Δdim-2 *strain gains cross-compartment contacts.*** (A,C) Heatmaps of raw (above
783 diagonal) or KR-corrected (below diagonal) contact probability changes across LG II in a Δ*cdp-2*;Δ*dim-2 Dpn*II
784 *in situ* Hi-C dataset relative to (A) WT or (C) Δ*cdp-2* datasets. Arrowheads indicate the heterochromatic
785 regions in panel D. (B) Quantification of strongly changed intra-chromosomal (top) or inter-chromosomal
786 (bottom) contacts in Δ*cdp-2* or Δ*cdp-2*;Δ*dim-2* datasets relative to a WT dataset, as in Figure 1E. (D) Heatmap
787 of the raw contact probability changes of two heterochromatic regions in a Δ*cdp-2*;Δ*dim-2* strain relative to
788 (top) WT or (bottom) Δ*cdp-2* strains. IGV image of Δ*cdp-2* or Δ*cdp-2*;Δ*dim-2* H3K9me3 enrichment is in the
789 middle.
790
791 ***Figure 6. Models for how HCHC loss impacts heterochromatin formation and genome organization in***
792 **Neurospora crassa*.*** (A-D) For WT or HCHC mutant strains, heterochromatin formation at nucleosomes
793 (left) and the organization of two example chromosomes (right) are presented. (A) In a WT strain, the HCHC

794 (HDA-1, CDP-2, HP1, and CHAP) complex removes acetyl marks (green triangles) from histone tails. CDP-2
795 and HP1, which binds H3K9me3 (red hexagons) while CHAP binds AT-rich DNA (orange lines) between
796 distant nucleosomes to recruit HDA-1. The DCDC (DIM-5/7/9, CUL4, DDB1^{dim-8}, Complex) tri-methylates
797 H3K9 on deacetylated histone tails, and HP1 binds H3K9me3 to directly recruit the DNA methyltransferase
798 DIM-2 for cytosine methylation (orange hexagons). The activity of both HCHC and DCDC establishes the Rabl
799 chromosome conformation characterized by a centromere (red circles) cluster distinct from (sub)telomeres
800 bundles (green circles) and the clustering of interspersed heterochromatic regions (black circles), all of
801 which occur at the nuclear periphery. (B) CDP-2 loss increases heterochromatic histone acetylation and
802 alters (here, gains) 5^{m}C while maintaining H3K9me3 at most AT-rich loci, which together increases intra-
803 heterochromatic region contacts and decreases inter-chromosomal centromeric contacts. (C) CHAP loss
804 relaxes heterochromatic region compaction and reduces inter-heterochromatic region interactions, despite
805 increases in 5^{m}C and H3K9me3. (D) Loss of both CDP-2 and DIM-2 increases histone acetylation, H3K9me3
806 enrichment, and genome disorder as heterochromatic regions amalgamate with euchromatin.

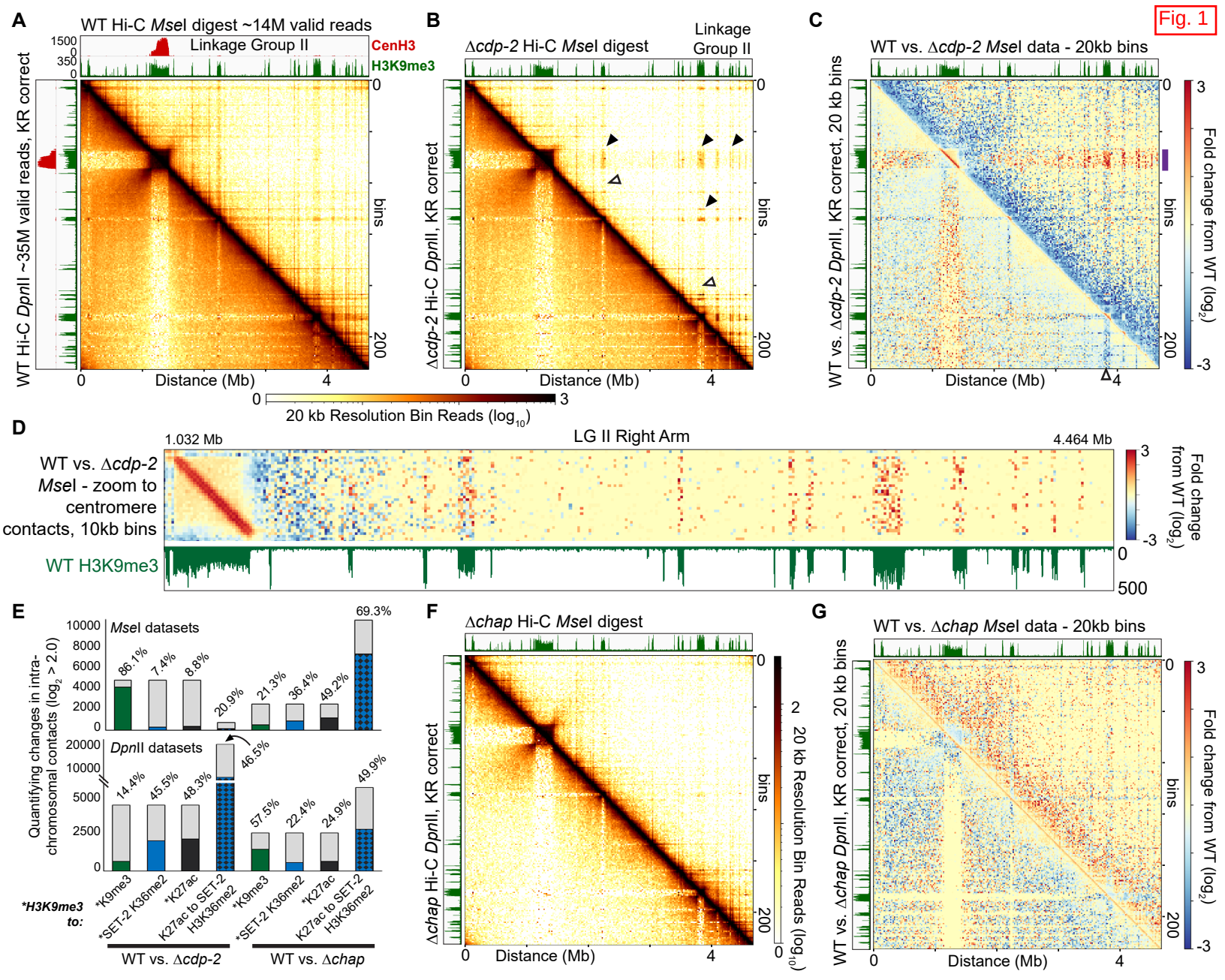
Fig. 1
A
WT Hi-C MseI digest ~14M valid reads
Linkage Group II
CenH3
H3K9me3
WT Hi-C DpnII ~35M valid reads, KR correct
bins
Distance (Mb)
B
Δcdp-2 Hi-C MseI digest
Linkage Group II
Δcdp-2 Hi-C DpnII, KR correct
C
WT vs. Δcdp-2 MseI data - 20kb bins
WT vs. Δcdp-2 DpnII, KR correct, 20 kb bins
Fold change from WT (log2)
20 kb Resolution Bin Reads (log10)
D
LG II Right Arm
1.032 Mb
4.464 Mb
WT vs. Δcdp-2 MseI - zoom to centromere contacts, 10kb bins
WT H3K9me3
Fold change from WT (log2)
E
MseI datasets
DpnII datasets
Quantifying changes in intra-chromosomal contacts (log2 > 2.0)
86.1%
7.4%
8.8%
20.9%
21.3%
36.4%
49.2%
69.3%
14.4%
45.5%
48.3%
46.5%
57.5%
22.4%
24.9%
49.9%
*H3K9me3 to:
*K9me3
*SET-2 K36me2
*K27ac
K27ac to SET-2 H3K36me2
WT vs. Δcdp-2
WT vs. Δchap
F
Δchap Hi-C MseI digest
Δchap Hi-C DpnII, KR correct
20 kb Resolution Bin Reads (log10)
G
WT vs. Δchap MseI data - 20kb bins
WT vs. Δchap DpnII, KR correct, 20 kb bins
Fold change from WT (log2)

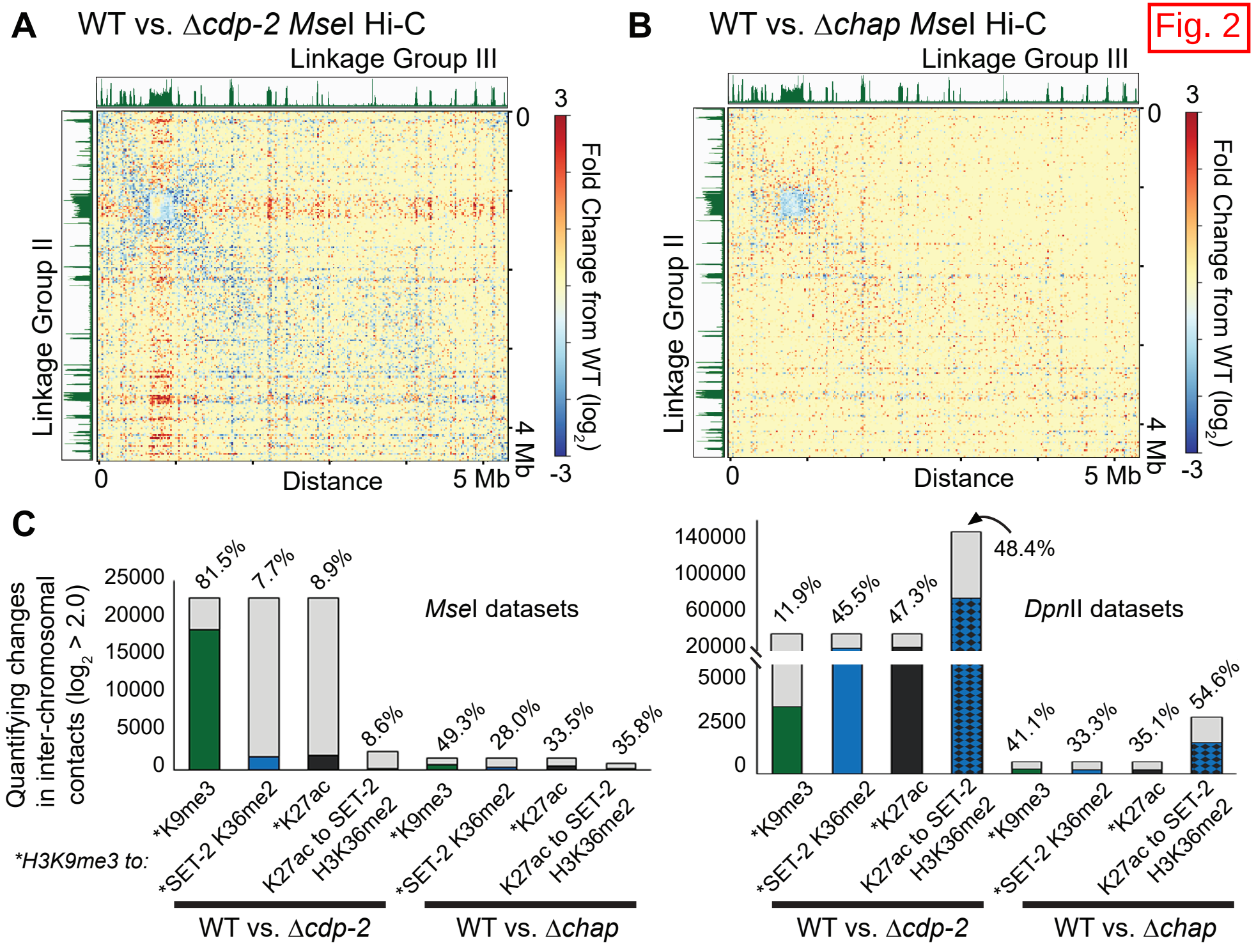
Fig. 2
A
WT vs. Δcdp-2 MseI Hi-C
Linkage Group III
Linkage Group II
Distance
0
5 Mb
4 Mb
3
-3
Fold Change from WT (log2)
B
WT vs. Δchap MseI Hi-C
Linkage Group III
Linkage Group II
Distance
0
5 Mb
4 Mb
3
-3
Fold Change from WT (log2)
C
Quantifying changes in inter-chromosomal contacts (log2 > 2.0)
MseI datasets
81.5%
7.7%
8.9%
8.6%
49.3%
28.0%
33.5%
35.8%
*K9me3
*SET-2 K36me2
*K27ac
K27ac to SET-2 H3K36me2
*H3K9me3 to:
WT vs. Δcdp-2
WT vs. Δchap
DpnII datasets
11.9%
45.5%
47.3%
48.4%
41.1%
33.3%
35.1%
54.6%

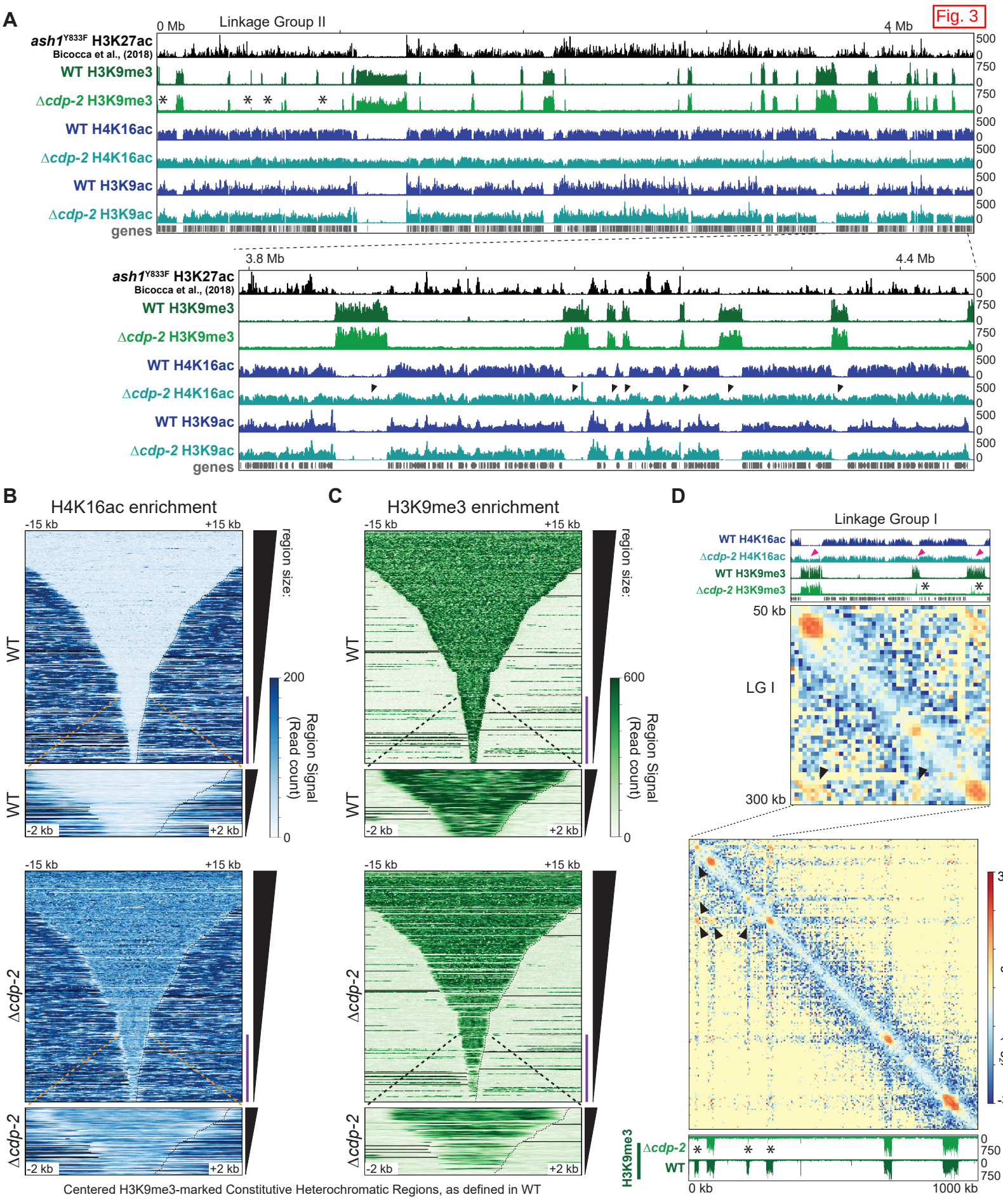
Fig. 3
A
Linkage Group II
0 Mb
4 Mb
ash1Y833F H3K27ac
Bicocca et al., (2018)
WT H3K9me3
Δcdp-2 H3K9me3
WT H4K16ac
Δcdp-2 H4K16ac
WT H3K9ac
Δcdp-2 H3K9ac
genes
3.8 Mb
4.4 Mb
B
H4K16ac enrichment
-15 kb
+15 kb
region size:
WT
Δcdp-2
200
0
Region Signal (Read count)
-2 kb
+2 kb
C
H3K9me3 enrichment
600
D
Linkage Group I
50 kb
LG I
300 kb
Fold change from WT (log2)
3
-3
H3K9me3
0 kb
1000 kb
Centered H3K9me3-marked Constitutive Heterochromatic Regions, as defined in WT

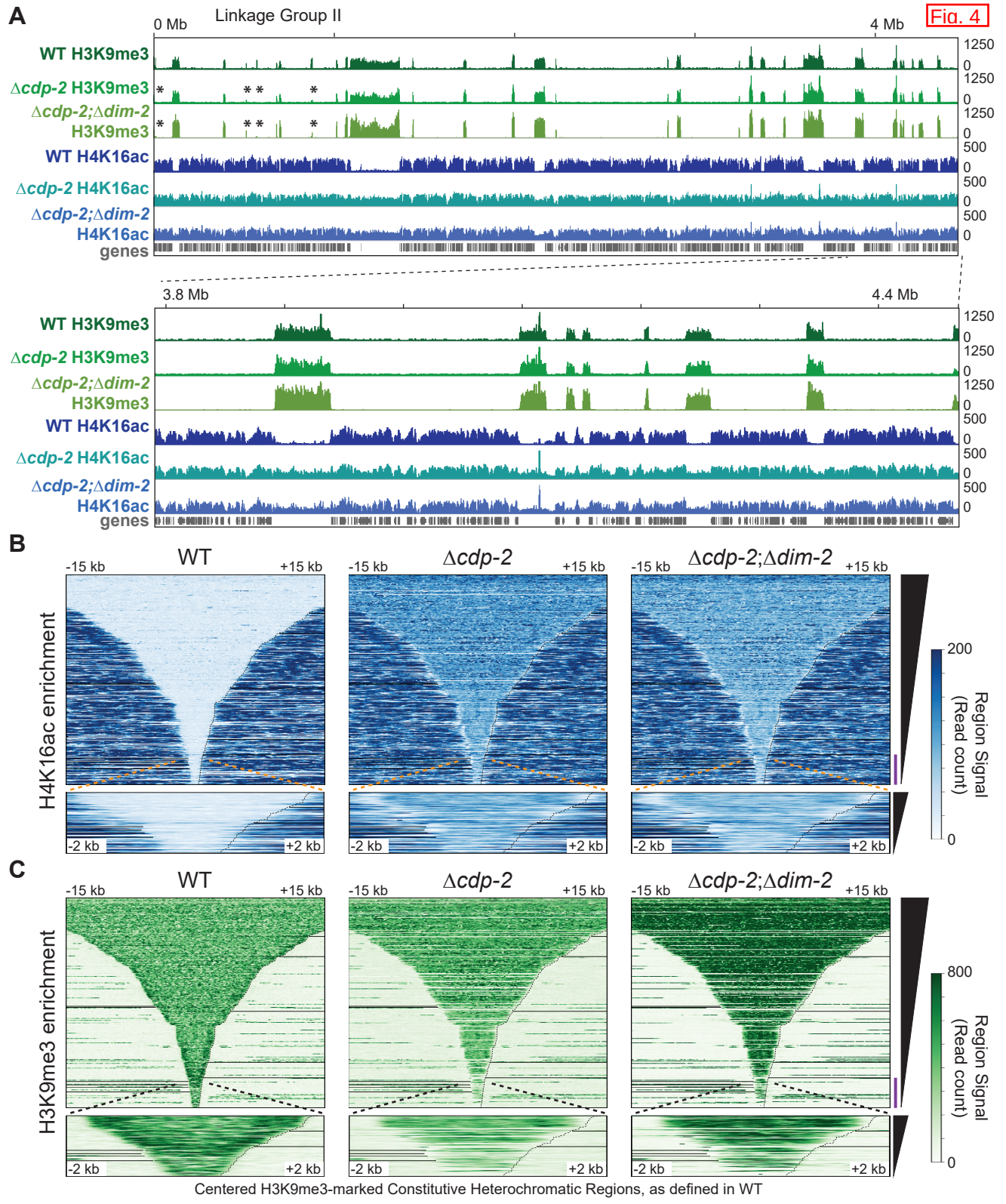
Fig. 4
A
Linkage Group II
0 Mb
4 Mb
WT H3K9me3
Δcdp-2 H3K9me3
Δcdp-2;Δdim-2 H3K9me3
WT H4K16ac
Δcdp-2 H4K16ac
Δcdp-2;Δdim-2 H4K16ac
genes
1250
500
0
3.8 Mb
4.4 Mb
B
WT
Δcdp-2
Δcdp-2;Δdim-2
-15 kb
+15 kb
-2 kb
+2 kb
H4K16ac enrichment
200
Region Signal (Read count)
C
H3K9me3 enrichment
800
Centered H3K9me3-marked Constitutive Heterochromatic Regions, as defined in WT

Fig. 5

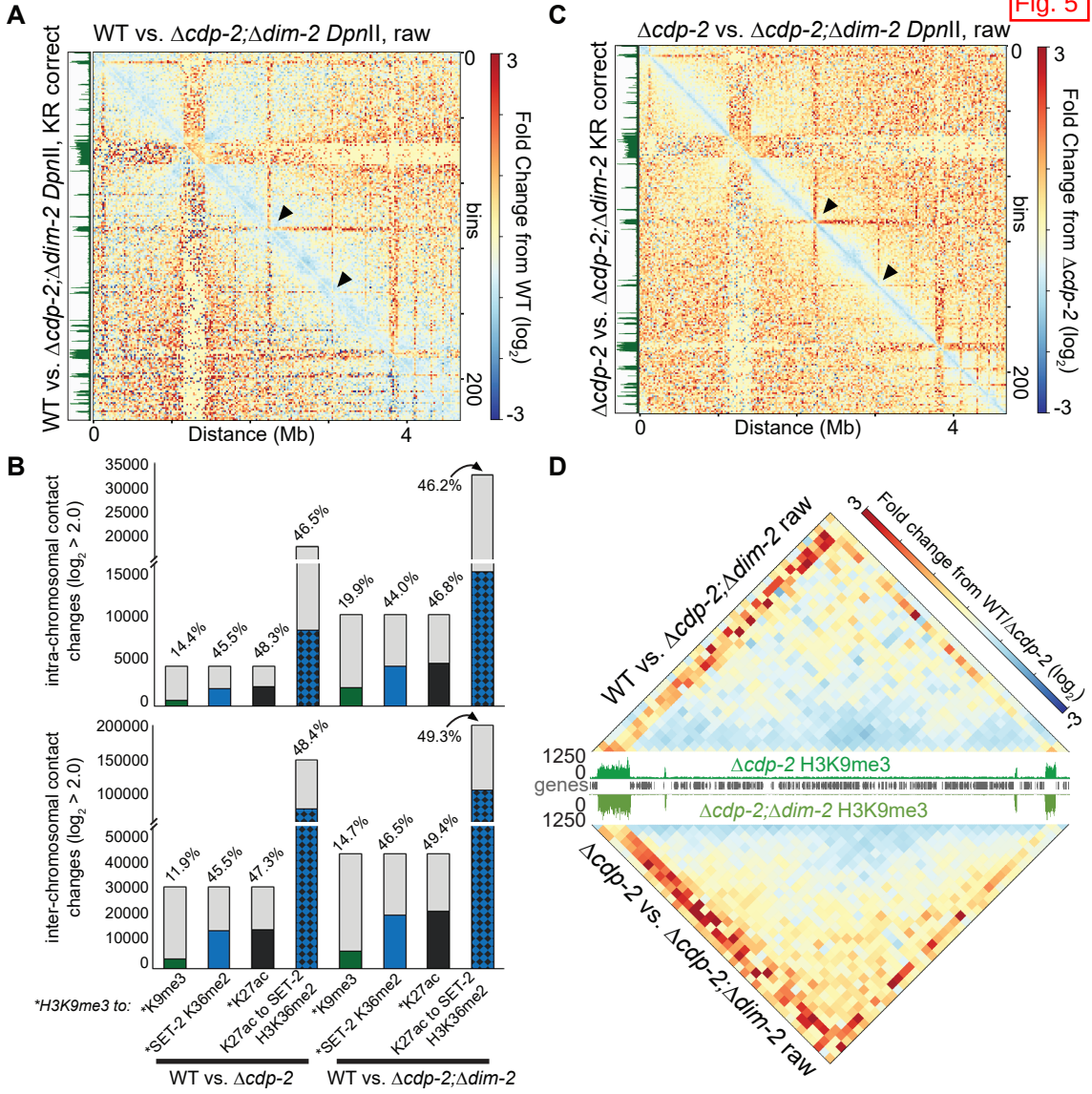
A
WT vs. Δcdp-2;Δdim-2 DpnII, raw
WT vs. Δcdp-2;Δdim-2 DpnII, KR correct
bins
Distance (Mb)
Fold Change from WT (log2)
C
Δcdp-2 vs. Δcdp-2;Δdim-2 DpnII, raw
Δcdp-2 vs. Δcdp-2;Δdim-2 KR correct
Fold Change from Δcdp-2 (log2)
B
intra-chromosomal contact changes (log2 > 2.0)
inter-chromosomal contact changes (log2 > 2.0)
14.4%
45.5%
48.3%
46.5%
19.9%
44.0%
46.8%
46.2%
11.9%
45.5%
47.3%
48.4%
14.7%
46.5%
49.4%
49.3%
*H3K9me3 to:
*K9me3
*SET-2 K36me2
*K27ac
K27ac to SET-2 H3K36me2
WT vs. Δcdp-2
WT vs. Δcdp-2;Δdim-2
D
WT vs. Δcdp-2;Δdim-2 raw
Fold change from WT/Δcdp-2 (log2)
Δcdp-2 H3K9me3
genes
Δcdp-2;Δdim-2 H3K9me3
Δcdp-2 vs. Δcdp-2;Δdim-2 raw

Fig. 6

A

Wildtype heterochromatin and genome organization

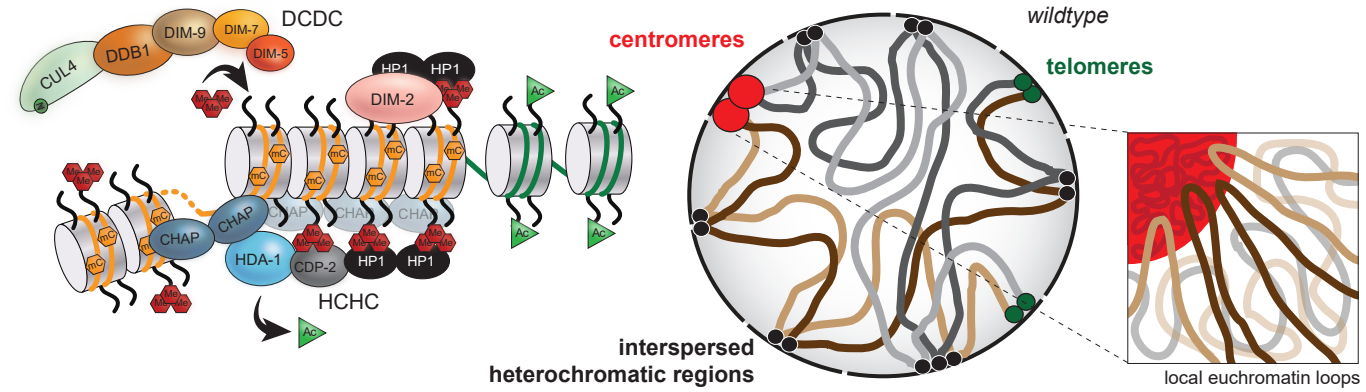

B

HCHC-deficient (Δ*cdp-2*) heterochromatin and genome organization

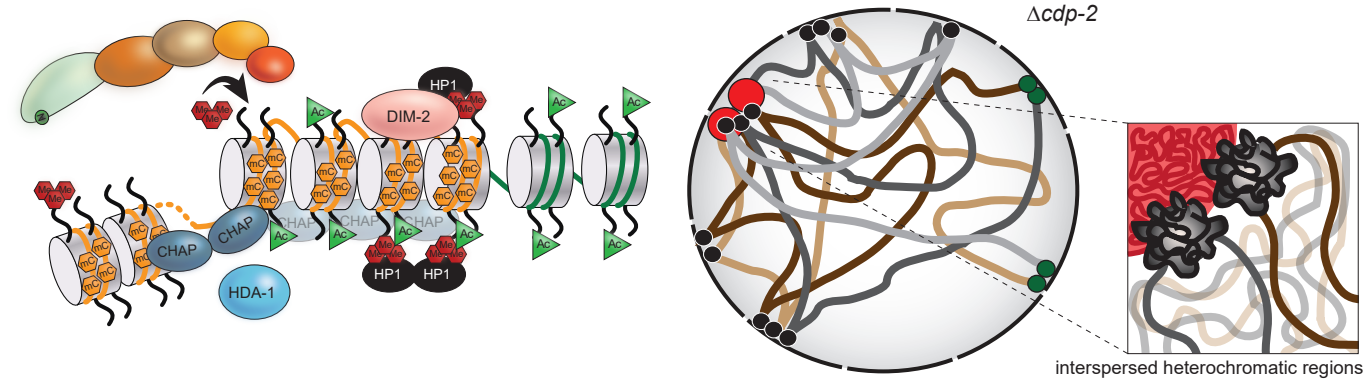

C

HCHC-deficient (Δ*chap*) heterochromatin and genome organization

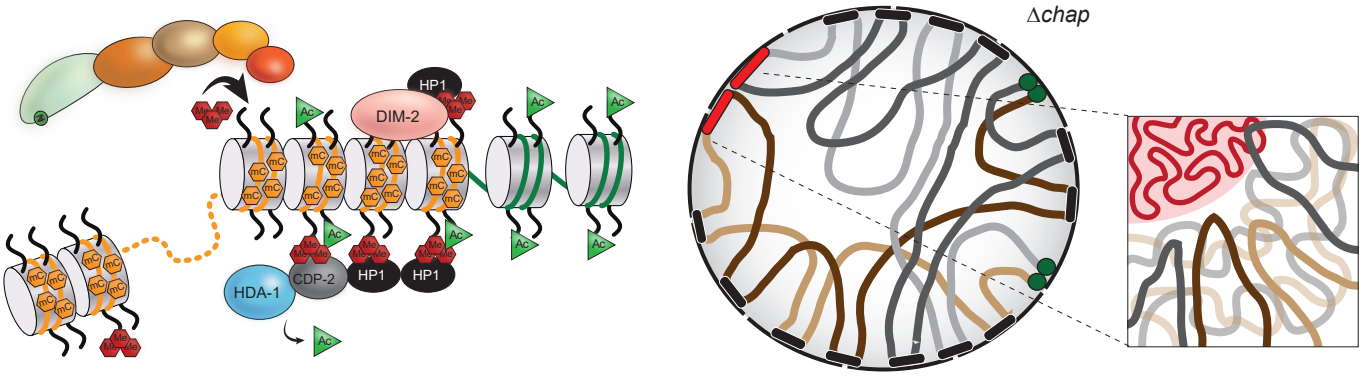

D
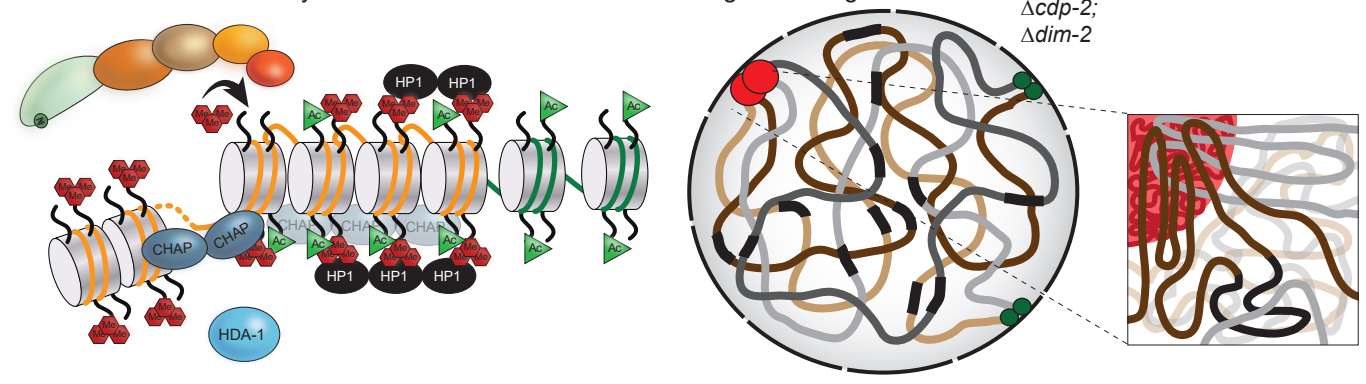
HCHC and DNA methylation-deficient heterochromatin and genome organization